processes

MDPI

Article

Separation of an Industrial Mixture of Decalin or Naphthalene Fluorination Products: Cis-Perfluorodecalin, Trans-Perfluorodecalin and Perfluoro(butylcyclohexane): Physicochemical, Thermophysical, and Spectral Data

Egor V. Lupachev *, Andrey A. Voshkin *, Alexey V. Kisel', Nikolai N. Kulov, Yulia A. Zakhodyaeva and Andrei V. Polkovnichenko *

Laboratory of Theoretical Foundations of Chemical Engineering, Kurnakov Institute of General and Inorganic Chemistry RAS, Moscow 119991, Russia; kisel.al@mail.ru (A.V.K.); kulov@igic.ras.ru (N.N.K.); yz.igic@gmail.com (Y.A.Z.)

* Correspondence: egorlu91@gmail.com (E.V.L.); voshkin@igic.ras.ru (A.A.V.); anzakhlevniy@rambler.ru (A.V.P.)

Abstract: New physicochemical data for trans-perfluorodecalin (trans-PDF) and cis-perfluorodecalin (cis-PFD) are presented. Based on the differential scanning calorimetry, the temperature and heat of the solid–liquid phase transition are determined. The coefficients of Antoine's equation are calculated based on the experimental temperature–pressure dependence data. This article also presents data on the rheological properties («zero» shear viscosity and apparent activation energy for the viscous flow) of the studied compounds. The dependencies of refractive index and excess volume (density) on temperature are studied. Gas chromatography–mass spectrometry data and FTIR, ^{13}C NMR, and ^{19}F NMR spectra are provided. The dependencies are given for the perfluoro(butylcyclohexane) (BCH)–trans-PFD, BCH–cis-PFD, and trans-PFD–cis-PFD binary systems and BCH–trans-PFD–cis-PFD ternary system: refractive index and density (liquid molar volume and excess molar volume) of composition and temperature. The dependences of the excess molar volume on the composition and temperature of the mixtures are correlated with Redlich-Kister and Kohler equations.

Keywords: trans-perfluorodecalin; cis-perfluorodecalin; perfluoro(butylcyclohexane); perfluorocycloalkanes; physicochemical data; saturated vapor pressure; density; refractive index; viscosity; excess molar volume

Citation: Lupachev, E.V.; Voshkin, A.A.; Kisel', A.V.; Kulov, N.N.; Zakhodyaeva, Y.A.; Polkovnichenko, A.V. Separation of an Industrial Mixture of Decalin or Naphthalene Fluorination Products: Cis-Perfluorodecalin, Trans-Perfluorodecalin and Perfluoro(butylcyclohexane): Physicochemical, Thermophysical, and Spectral Data. *Processes* **2023**, *11*, 3208. https://doi.org/10.3390/pr11113208

Academic Editor: Blaž Likozar

Received: 12 October 2023
Revised: 3 November 2023
Accepted: 8 November 2023
Published: 10 November 2023

1. Introduction

According to macroeconomic projections in the Perfluorocarbons Market—Global Industry Analysis and Forecast (2023–2029) [1], the perfluorocarbons market is expected to grow at a compound annual growth rate of 4.2% during the forecast period, reaching US$ 4.77 Bn by 2029. The report indicates that the perfluorocarbon (also called perfluoronaphthenes) application has facilitated the development of significantly more complex and faster processing semiconductors [1]. This will result in an increased demand for perfluorocarbons, considered major growth drivers for the market growth during the forecasted period. Meanwhile, application in the artificial photosynthesis process, which helps develop nanoemulsions for cancer detection, is attracting vendors. Perfluorocarbons are emerging in the healthcare sector and have been highly adopted in manufacturing as they help develop non-invasive imaging methodologies for assessing the potential efficacy of central nervous system transplantation of stem cells. Furthermore, development in the personal care and electronics sector is expected to serve as the primary growth factor for global perfluorocarbons in a calculated period. Semiconductor cleaning is a major

sector associated with its broad application and is, thus, broadly utilized to cover market value with significant growth.

The present research considers perfluorodecalin (PFD)–naphthalene, 1,1,2,2,3,3,4,4,4a,5,5,6,6,7,7,8,8,8a-octadecafluorodecahydro-. The history of PFD dates back to the 1940s. In the scientific literature, the over earlier mention of PFD application is associated with intravenous therapy [2]; until the 1990s, research on its use was mainly focused on blood substitution and oxygen carriers: oxygen-supply level after exchange blood-transfusion and liver function –mono-oxygenase system (cytochrome-P-450) microsomal cytochrome P-450-containing mono-oxygenase system [3–15]. PFD has also been considered as a matrix in spectroscopic studies [16], a chemical tracer to assess ocean models [17], and an aeration agent of the nutrient medium for tissue culture cell growth and mycobacteria culture [18,19].

An in-depth review of the scientific literature up to 2015 shown an active interest in PFD for myriad medical, biochemical, and chemical engineering side: blood substitute [20–24], liquid fluorocarbon lavage of airways [25–27], transplantology [28,29], extracorporeal life support [30], cryosurgery and tissue engineering [31–34], tattoos treatment [32,35–44], ophthalmology [45–55], drug production [56–60], headspace-gas chromatography-tandem [61] and electrospray ionization [62] mass spectrometry, magnetic resonance imaging oximetry [63], cell and microbial culturing [64–70], immersion medium [71–74], gas carrier and inert solvents [75–84], meso- and macro-mesoporous silica production [85], hydrogen production [86–88], and solar cell production [89].

Studies have also reported on various PFD properties: vapor pressure [90], phase data (LLE with hydrocarbon binary [91], ternary, etc. systems [92]); nucleation rate of gas hydrates [93,94], extraction [95], and gas solubility (liquid–gas partition-coefficients of halothane and isoflurane [96], N_2, N_2O, NH_3, O_2, and CO_2 [97–100]); density and viscosity [90,101–104]; surface properties (surface tension [104,105], interfacial tension against water [106], influence of pluronic F-68 dissolved in the aqueous phase [107], and wetting dynamics [108]); aqueous emulsions (preparation and physicochemical properties [109,110], effect of flocculation on particle enlargement [111]); adsorption properties [112] and aerodynamic diameter [113]; molecular structure and spectral properties (electron-diffraction of the gas phase structure [114], infrared spectra and radiative efficiency [115], NMR spectrum [63,116], conformation [117–120], and isomerization [121–124]); chemical and biological inertness of PFD [125–127]. Most data were obtained from a mixture of cis- and trans-PFD isomers (CAS No 306-94-5); many were not systematic and primarily related to PFD practical properties. Notably, the experimental data on the properties of PFD are especially relevant considering that the theoretical studies on the properties of fluorinated compounds are limited by the inability to apply the density functional theory (DFT) due to the relativistic effects and no overlap between the DFT exchange and exact exchange holes [128,129].

This article is a continuation of a series [130–134] on the separation and purification process of the constituents of the industrial system of close-boiling isomeric reaction products from the fluorination of decalin or naphthalene. The primary aim is to obtain physicochemical data on the properties of the cis- and trans-PFD isomers and their impurities: perfluoro(butylcyclohexane) (BCH). Note that physicochemical data on the pure substances and their mixtures are relatively absent from the literature. Such information is the foundation for developing separation/purification methods and is of significant scientific and industrial interest [130].

2. Materials and Methods

2.1. System and Its Component Data

The objects of this research are perfluoro-(butylcyclohexane), trans-perfluorodecalin, cis-perfluorodecalin (cis-PFD), and binary and ternary mixtures of these components. The considered components and their mixture are the constituents of an industrial system of

close-boiling geometric/configurational and structural/constitutional isomeric reaction products of the electrochemical fluorination of decalin or naphthalene [119,135,136]. Previously [130], we identified the main impurities of the reaction mixture (BCH and perfluoro(7-methylbicyclo[4.3.0]nonane) (MBCN)) and described the physicochemical properties of the BCH, MBCN and their binary mixture; the commercial value of BCH and MBCN was also discussed in previous works [130,131,133]. This study considers the BCH–trans-PFD–cis-PFD ternary constituent of the MBCN–BCH–trans-PFD–cis-PFD four-component industrial mixture.

The data on the compounds used are summarized in Table 1. BCH, cis- and trans-PFD were purified by distillation methods and crystallization. The purity of the reagents was confirmed by gas chromatography. The 1H NMR additionally analyzed the samples to determine the partially fluorinated impurity content.

Table 1. Specifications of the compounds used.

Chemical Name	CAS-No	Molar Mass M/g·mol^{-1}	Supplier	Initial Mass Fraction Purity	Purification Method	Mass Fraction after Purification (GC [a])
Perfluoro(butylcyclohexane)	374-60-7	500.07	P&M Invest	0.80–0.90	Heteroazeotropic distillation and crystallization	≥0.997
Trans-perfluorodecalin	60433-12-7	462.08	P&M Invest	0.80–0.90	Heteroazeotropic distillation, crystallization	≥0.998
Cis-perfluorodecalin	60433-11-6	462.08	P&M Invest	0.70–0.80	Heteroazeotropic distillation, crystallization	≥0.995

[a] Gas chromatography–flame ionization detector (Agilent 6890N equipped with a Restek RTX-1701 RK12054 capillary column).

2.2. Equipment and Analytics

The molecular weights of cis-PFD and trans-PFD were determined by gas chromatograph Maestro-αMS (INTERLAB, Moscow, Russia) with a quadrupole mass spectrometer (capillary column SCI-5MS-025-025-30, UVISON, Sevenoaks, UK; vaporizer temperature (injection port temperature), 200 °C; column (oven) temperature, 40 °C (3 min); ionization energy, 70 eV; detector: scan mode, (m·z^{-1} 50–550); interface temperature, 250 °C; ion source temperature, 230 °C; carrier gas–helium 1 mL·min^{-1}).

The Bruker AVANCE-300 radio spectrometer (Bruker, Billerica, MA, USA) and IRTracer-100 Spectrophotometer (Shimadzu, Kyoto, Japan) were used to obtain the nuclear magnetic resonance (NMR) and Fourier transform infrared (FTIR) spectra (Sigma-Aldrich St. Louis, MO, USA), respectively. Differential scanning calorimetry (DSC) was employed to determine the temperature and heat of the solid−liquid phase transition (METTLER TOLEDO DSC 3+, Mettler Toledo, Columbus, OH, USA). Rotational rheometry was used to study rheological properties (Anton Paar Physica MCR301 rheometer (Geminibv, Apeldoorn, Netherlands); stationary flow conditions). The Abbemat 3200 refractometer (Fisher Scientific, Hampton, NH, USA) and DMA 1001 densimeter (Anton Paar, Sumida City, Japan) were applied to measure refractive index, n_D, and density, ρ, respectively. A detailed description of the equipment and modes were described previously [130].

Mass Comparator MC-1000 (A&D Company, Limited Toshima City, Japan) was used to measure sample weight, m. Mercury "Mereno pri ponoru" thermometers and a vacuum meter VACUU VIE extended were also employed to measure temperature, T, and pressure, P, respectively.

2.3. Saturated Vapor Pressure Measurements

The saturated vapor pressure, P, was determined using the apparatus shown in Figure 1. The unit was hooded in a jacket to prevent partial condensation of vapors on the flask walls. After a constant pressure was set, the sample was brought to a boil with

continuous stirring (UT 4100S heating mantle (Trulia, San Francis, CA, USA) was used). The vapor phase produced in still *1* was condensed in the backflow condenser *2* and fed back to still *1*. The vapor, T_D, and liquid, T_W, phase temperatures were measured using thermometers *3* and *4*, respectively. The values were recorded once the parameters (*T*, *P*) were constant for 30 min. This was repeated three times for each experiment. The methodology was previously validated with distilled water [130] and is similar to a previously published protocol [137].

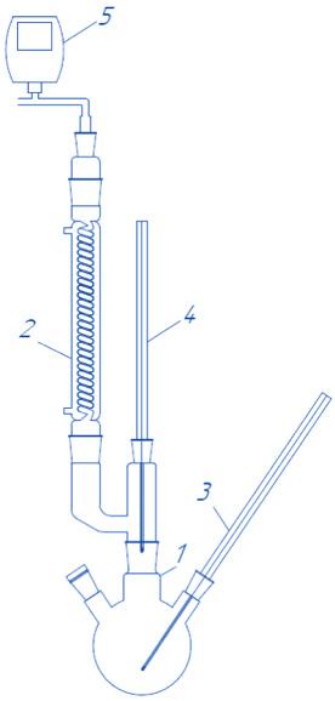

Figure 1. Apparatus for determining saturated vapor pressure: *1*—still; *2*—backflow condenser; *3* and *4*—thermometers; *5*—manometer. Reproduced from ref. [130]. Copyright 2023 American Chemical Society.

3. Results

3.1. Gas Chromatography–Mass Spectrometry Data

The gas chromatography–mass spectrometry (GC–MS) data for trans-PFD and cis-PFD are shown in Figure 2.

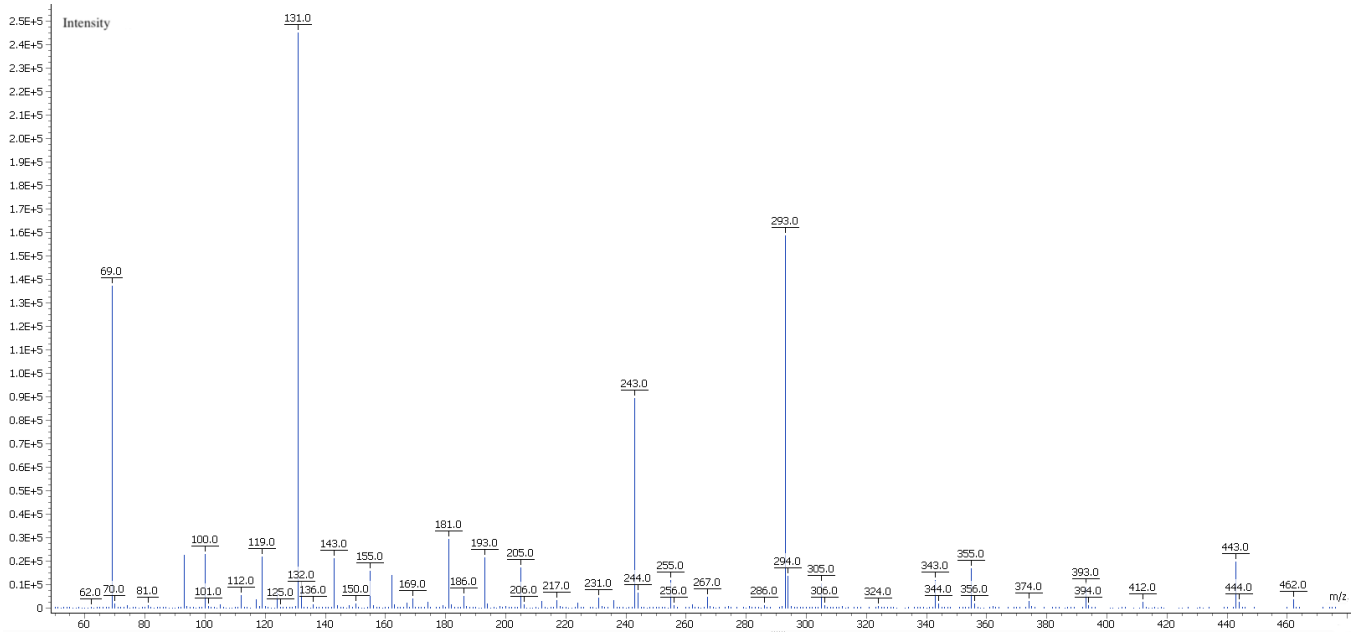

(**a**)

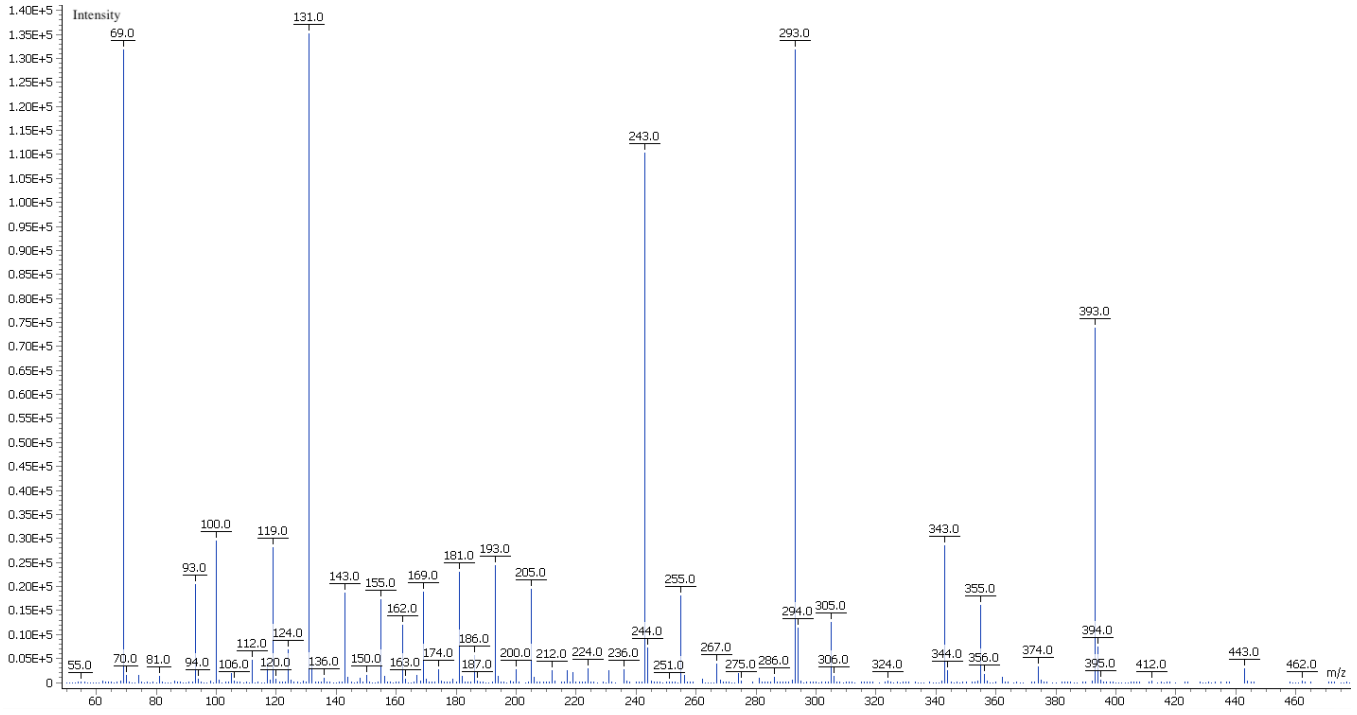

(**b**)

Figure 2. GC-MS data: (**a**) trans-perfluorodecalin; (**b**) cis-perfluorodecalin.

3.2. NMR and FTIR Spectra

The NMR (^{13}C and ^{19}F) and FTIR spectra for trans-PFD and cis-PFD are shown in Figures 3 and 4, respectively.

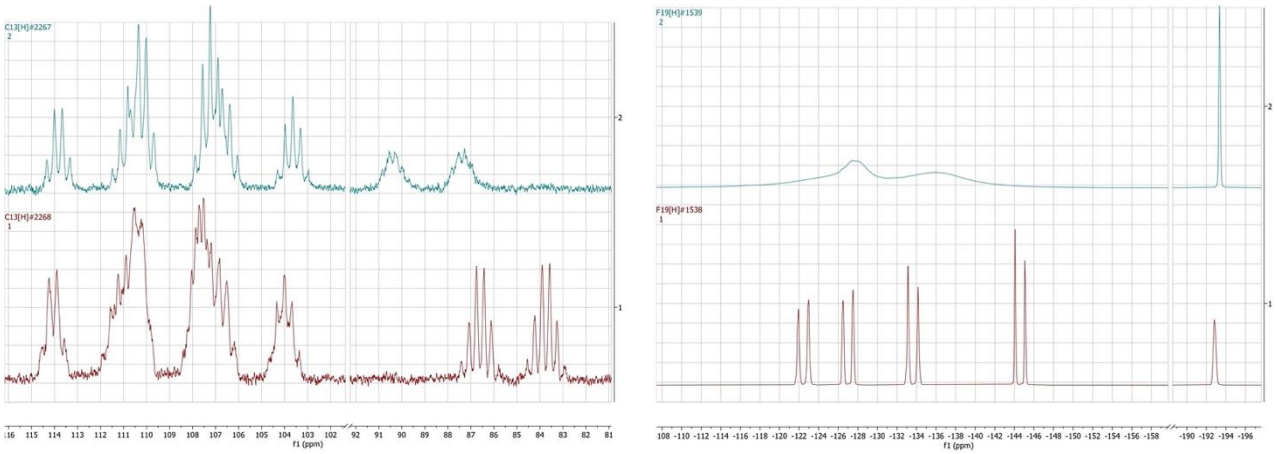

(**a**) (**b**)

Figure 3. NMR spectrum of trans-perfluorodecalin (red color) and cis-perfluorodecalin (blue color). (**a**) ^{13}C; (**b**) ^{19}F.

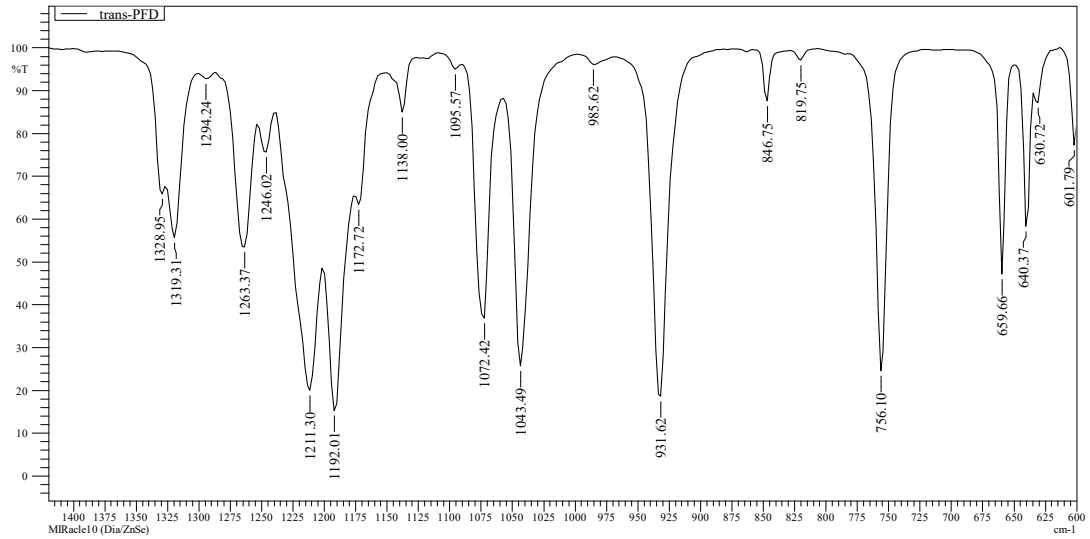

(**a**)

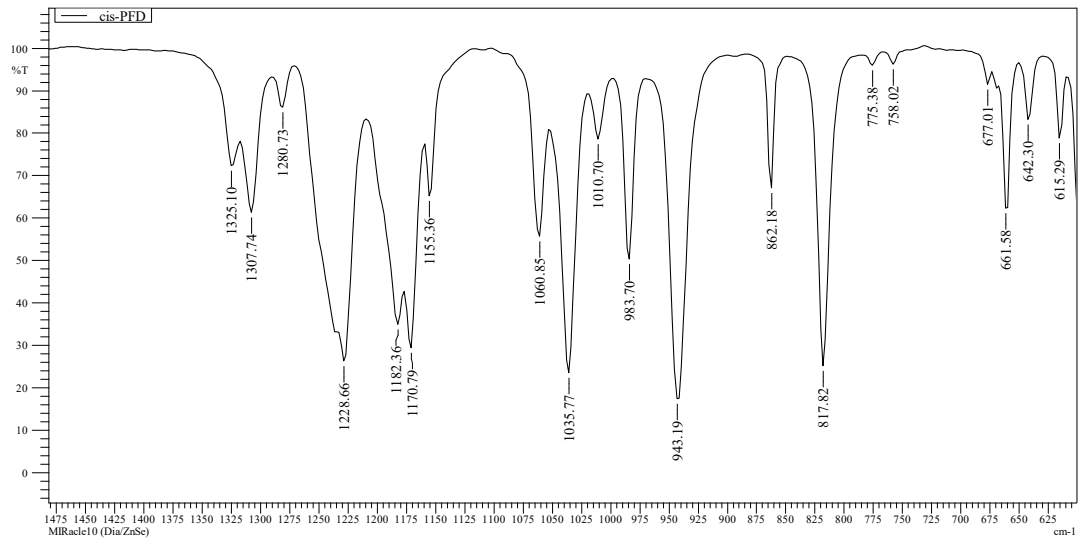

(**b**)

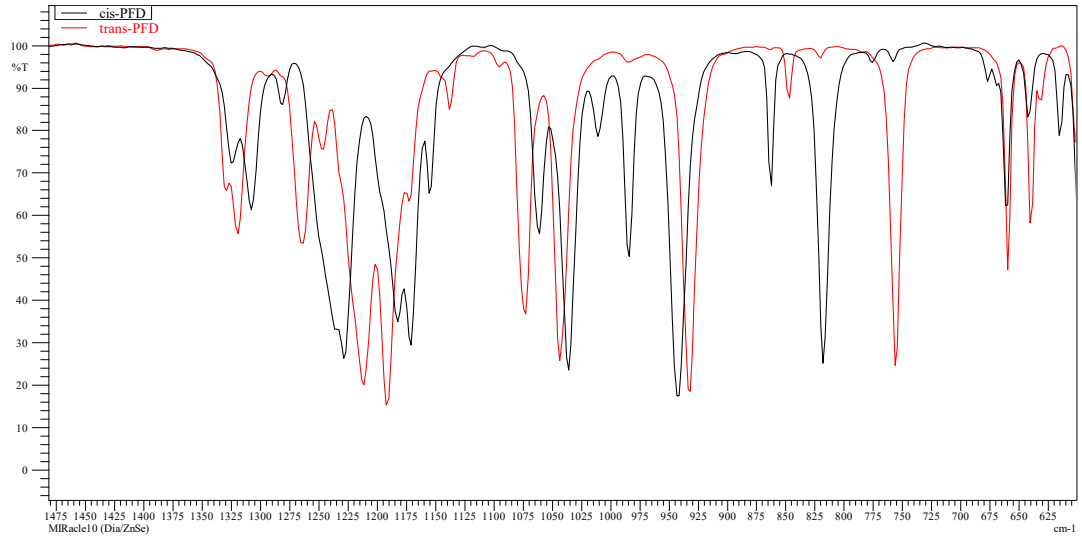

(**c**)

Figure 4. FTIR spectra. Fingerprint region of (**a**) trans-perfluorodecalin, (**b**) cis-perfluorodecalin, (**c**) spectra comparison (black—cis-PFD; red—trans-PFD).

3.3. Solid-Liquid Phase Transition

The DSC thermal transition data at a heating/cooling rate 10 °C·min^{-1} are presented in Figure 5. The data is presented as cooling and heating lines of the weighted samples. All of the heat flow effects are summarized in Table 2.

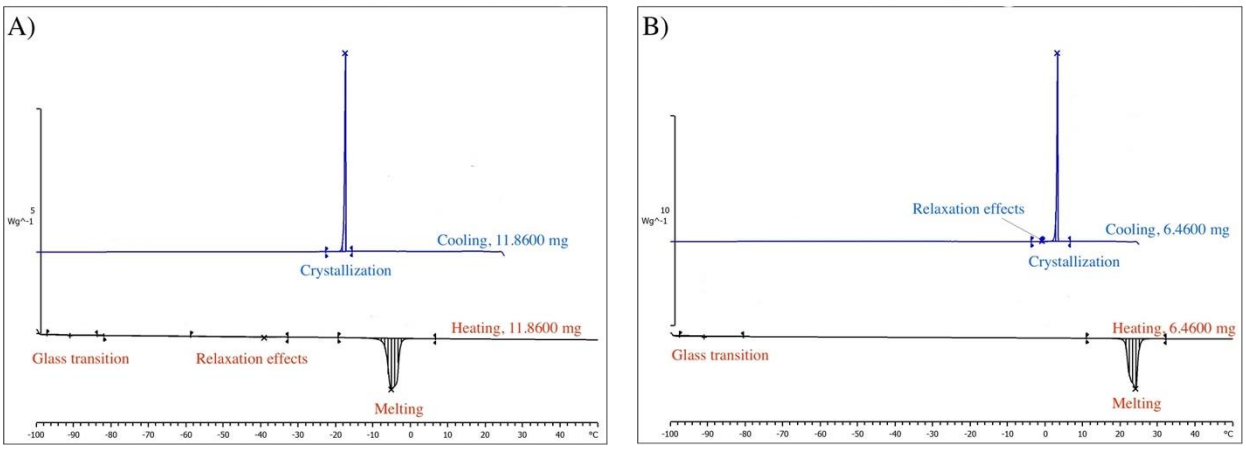

Figure 5. DSC scans. (**A**) cis-perfluorodecalin; (**B**) trans-perfluorodecalin.

Table 2. Differential scanning calorimetry data for cis-perfluorodecalin (cis-PFD) and trans-perfluorodecalin (trans-PFD) at sample mass m, temperature T, enthalpy H, heat capacity change ΔC_p, and pressure P = 98.3 kPa according to Figure 5 [a].

Component	**Cis-PFD**				**Trans-PFD**			
m/g·10^{-3}	11.8600				6.4600			
type	**cooling**	**heating**			**cooling**		**heating**	
Integral/mJ	−244.13	-	7.08	253.24	−233.17	0.65	-	248.15
normalized H/J·g^{-1}	−20.58	-	0.60	21.35	−36.09	0.10	-	38.41
ΔC_p/J·g^{-1}·K^{-1}	-	36.930 × 10^{-3}	-	-	-	-	49.199 × 10^{-3}	-
onset T/°C	−17.20	−95.69	-	−6.99	3.48	−0.74	−96.57	21.22
peak/average point T/°C	−16.24	−90.94	−39.11	−5.44	4.67	−0.90	−90.93	23.55
endset T/°C	−17.65	−87.60	-	−2.88	3.13	−1.26	−85.87	24.95
Effect	crystallization	glass transition	solid-solid transition	melting	crystallization	relaxation	glass transition	melting

[a] Standard uncertainties u: u(m) = 0.01 g·10^{-3}; $u(T)$ = 0.25 °C; u_r(heat flow) = 0.05; $u(P)$ = 0.3 kPa.

3.4. Viscosity

Dependences of shear viscosity η on shear rate $\dot{y}$ at different temperatures for trans-PFD and cis-PFD are shown in Figure 6.

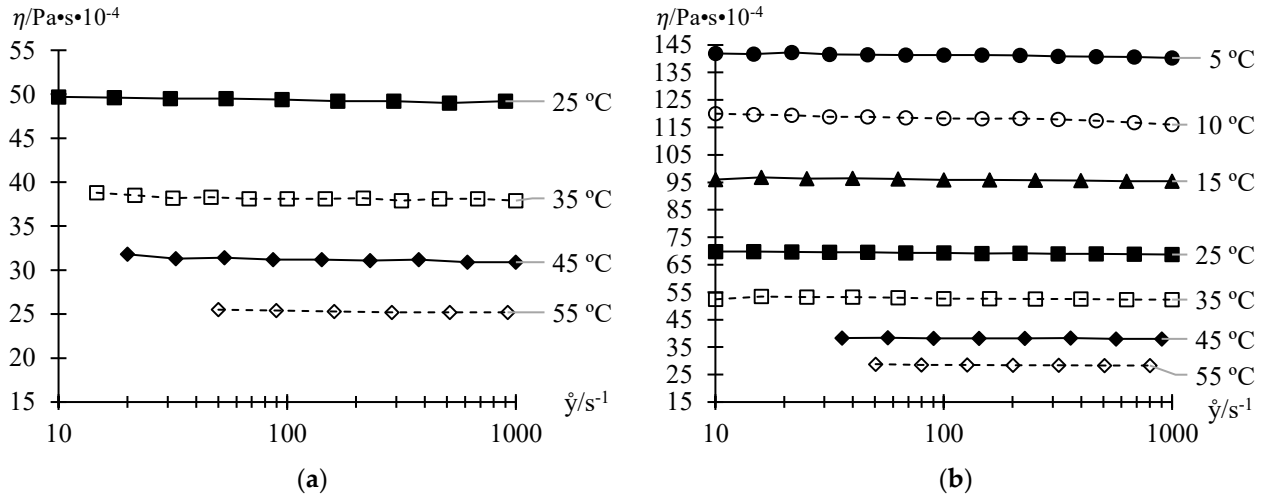

Figure 6. Dependences of shear viscosity η on shear rate $\dot{y}$ at different temperatures T. (**a**) Trans-perfluorodecalin; (**b**) cis-perfluorodecalin. Uncertainties: $u(T)$ = 0.2 °C; $u_r(\eta)$ = 0.02.

Experimental data on the dependences of «zero» shear viscosity on temperature for trans-PFD and cis-PFD are listed in Table 3 and Figure 7.

Table 3. Dependences of «zero» shear viscosity η on temperature T for trans-perfluorodecalin (trans-PFD) and cis-perfluorodecalin (cis-PFD) at pressure P = 99.3 kPa [a].

***T*/°C**	**5.0**	**10.0**	**15.0**	**25.0**	**35.0**	**45.0**	**55.0**
Component	***η*/Pa·s·10^{-4}**						
trans-PFD	-	-	-	49.4	38.2	31.2	25.3
cis-PFD	141.3	118.3	96.0	69.3	52.7	38.2	28.5

[a] Standard uncertainties u: $u(T)$ = 0.2 °C; $u_r(\eta)$ = 0.02; $u(P)$ = 0.3 kPa.

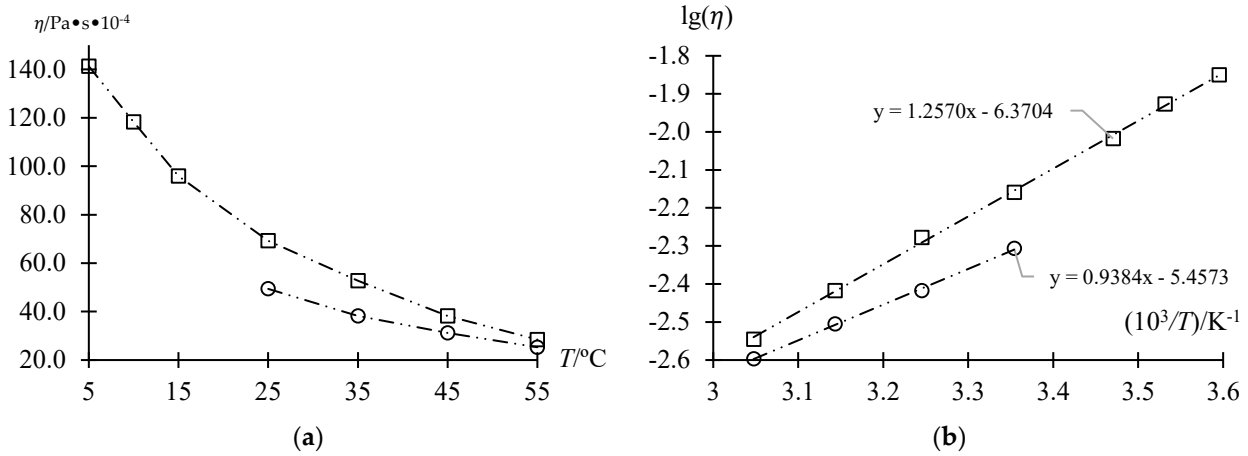

Figure 7. Dependences of «zero» shear viscosity η on temperature T according to Table 3. (**a**) $\eta = f(T)$; (**b**) $\lg(\eta) = f(10^3/T)$. Square—cis-perfluorodecalin; circle—trans-perfluorodecalin.

The dependences of the «zero» shear viscosity η of trans-PFD and cis-PFD on temperature T are described by the Arrhenius Equation (1):

$$\lg(\eta) = \lg(\eta_0) - E_a/(2.3 \cdot RT) \quad (1)$$

where η is «zero» shear viscosity, Pa·s; η_0 is a constant parameter, Pa·s; E_a represents the apparent activation energy for the viscous flow, J·mol^{-1}; R = 8.314 is the molar gas constant, J·K^{-1}·mol^{-1}; T represents temperature, K. The coefficients of the equation are listed in Table 4.

Table 4. Arrhenius Equation (1) coefficients.

Component	η_0/Pa·s· 10^{-6}	E_a/J·mol^{-1}
trans-perfluorodecalin	3.489	−17,944.3
cis-perfluorodecalin	0.426	−24,036.6

The trans-PFD cooling data up to the crystallization point are shown in Figure 8. The cooling rate was 1 °C·min^{-1}. The measurements were carried out at a shear rate of $\dot{\gamma}$ = 30 s^{-1}.

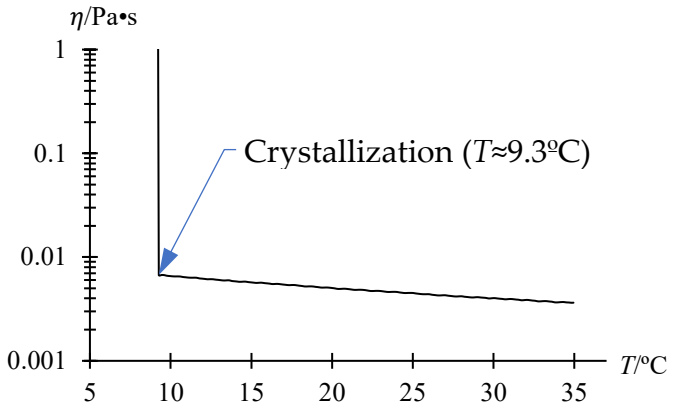

Figure 8. The dependence of shear viscosity of trans-PFD on temperature.

Figure 9 shows summary plots of shear viscosity versus shear rate at 25 °C. Additionally, the temperature dependences of viscosity are presented for the MBCN–BCH–trans-PFD–cis-PFD industrial system components of close-boiling isomeric reaction products for the electrochemical fluorination of decalin or naphthalene.

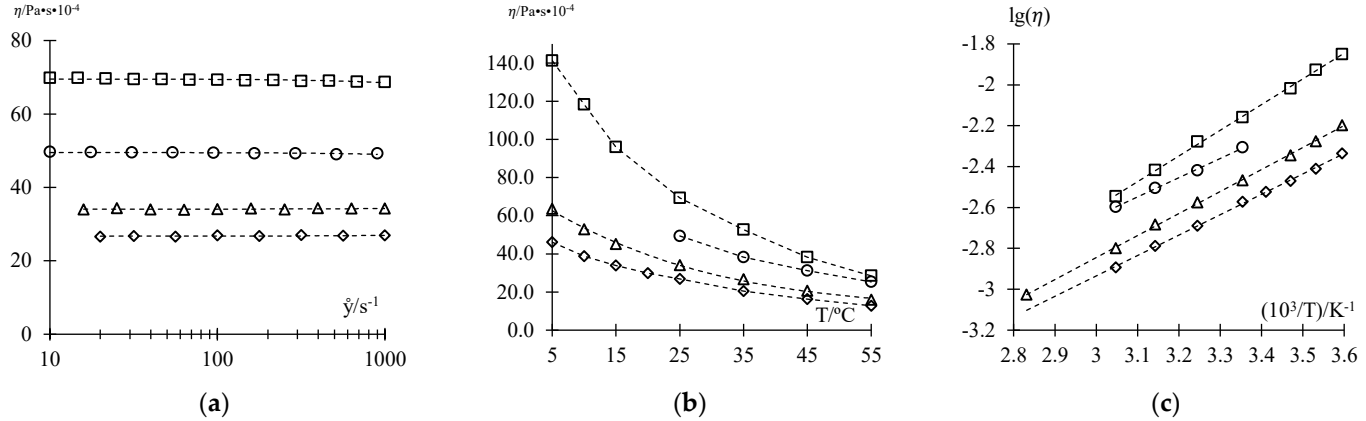

Figure 9. Viscosity data for constituents of the industrial system of the close-boiling isomeric reaction products for the electrochemical fluorination of decalin or naphthalene. (**a**) $\eta = f(\hat{y})$ at 25 °C; (**b**) $\eta = f(T)$; (**c**) $\lg(\eta) = f(1/T)$. Experimental data (Figure 6 and Table 3): circle—trans-perfluorodecalin; square—cis-perfluorodecalin. Literature data [130]: triangular—perfluoro(7-methylbicyclo[4.3.0]nonane); diamond—perfluoro(butylcyclohexane).

3.5. Dependence of the Boiling Temperature on Pressure

Dependence of the saturated vapor pressure, P, of trans-PFD and cis-PFD on temperature T was obtained on the unit depicted in Figure 1; experimental data are listed in Tables 5 and 6.

Table 5. Experimental saturated vapor pressure P data for trans-perfluorodecalin at temperature T [a].

T/°C	*P*/kPa	*T*/°C	*P*/kPa	*T*/°C	*P*/kPa	*T*/°C	*P*/kPa
66.0	6.3	102.0	28.2	120.4	51.6	134.3	77.7
74.1	9.2	105.0	31.2	122.1	54.4	136.0	81.7
83.1	13.6	107.3	33.8	123.9	57.3	137.7	85.2
86.6	15.6	109.4	36.1	125.2	59.8	139.2	89.1
89.9	17.7	112.1	39.6	126.6	62.1	140.9	93.2
92.2	19.5	114.2	42.4	128.2	65.3	142.1	96.3
94.1	21.0	114.7	42.8	129.9	68.4	143.5	100.1
96.0	22.5	116.2	45.2	131.0	71.0	-	-
97.5	23.9	118.0	47.6	132.5	73.9	-	-
99.0	25.3	118.9	48.9	133.1	75.4	-	-

[a] Standard uncertainties u are: $u(T) = 0.5$ °C; $u(P) = 0.3$ kPa.

Table 6. Experimental saturated vapor pressure P data for cis-perfluorodecalin at temperature T [a].

T/°C	*P*/kPa	*T*/°C	*P*/kPa	*T*/°C	*P*/kPa	*T*/°C	*P*/kPa
78.3	10.1	105.7	30.2	118.0	45.5	137.0	81.3
80.0	11.1	106.4	31.2	119.0	47.6	138.9	85.8
90.9	17.2	106.8	31.4	119.7	48.5	140.0	88.8
93.2	19.5	107.2	32.1	120.7	49.9	141.1	91.9
96.0	21.1	108.0	33.2	122.6	53.3	142.0	94.2
98.6	23.4	110.0	35.2	124.6	56.6	142.7	95.7
100.5	25.0	112.1	38.1	127.0	60.9	143.0	96.4
103.0	27.3	114.4	41.0	129.9	66.1	144.8	100.2
104.8	29.2	116.1	43.4	131.9	70.0	-	-
105.0	29.6	117.0	45.1	135.2	77.6	-	-

[a] Standard uncertainties u: $u(T) = 0.5$ °C; $u(P) = 0.3$ kPa.

The dependences of the saturated vapor pressure for trans-PFD and cis-PFD on temperature are described by the Antoine Equation (2):

$$lnP_i = A_i^P + \frac{B_i^P}{T + C_i^P} \quad (2)$$

where P is pressure, kPa; T is temperature, °C; A_i^P, B_i^P, and C_i^P represent coefficients of the Antoine equation. The regressed coefficients of the Antoine equation are presented in Table 7.

Table 7. Antoine Equation (2) coefficients for the temperature range [T_{min}, T_{max}].

Component	A_i^P	B_i^P	C_i^P	[T_{min}, T_{max}]/°C
trans-PFD	12.4765	−2350.0059	155	[66, 145]
cis-PFD	12.3477	−2248.9361	146	[78, 144]
BCH [130]	13.5630	−2900.7119	180	[80, 145]
MBCN [130]	13.5734	−2916.7343	190	[75, 145]

The correlation between the data calculated by the Antoine equation (Table 7) and those obtained experimentally (Tables 5 and 6) for saturated vapor pressure versus temperature is presented in the Figure 10; previously reported data [130] for MBCN and BCH are also provided for comparison.

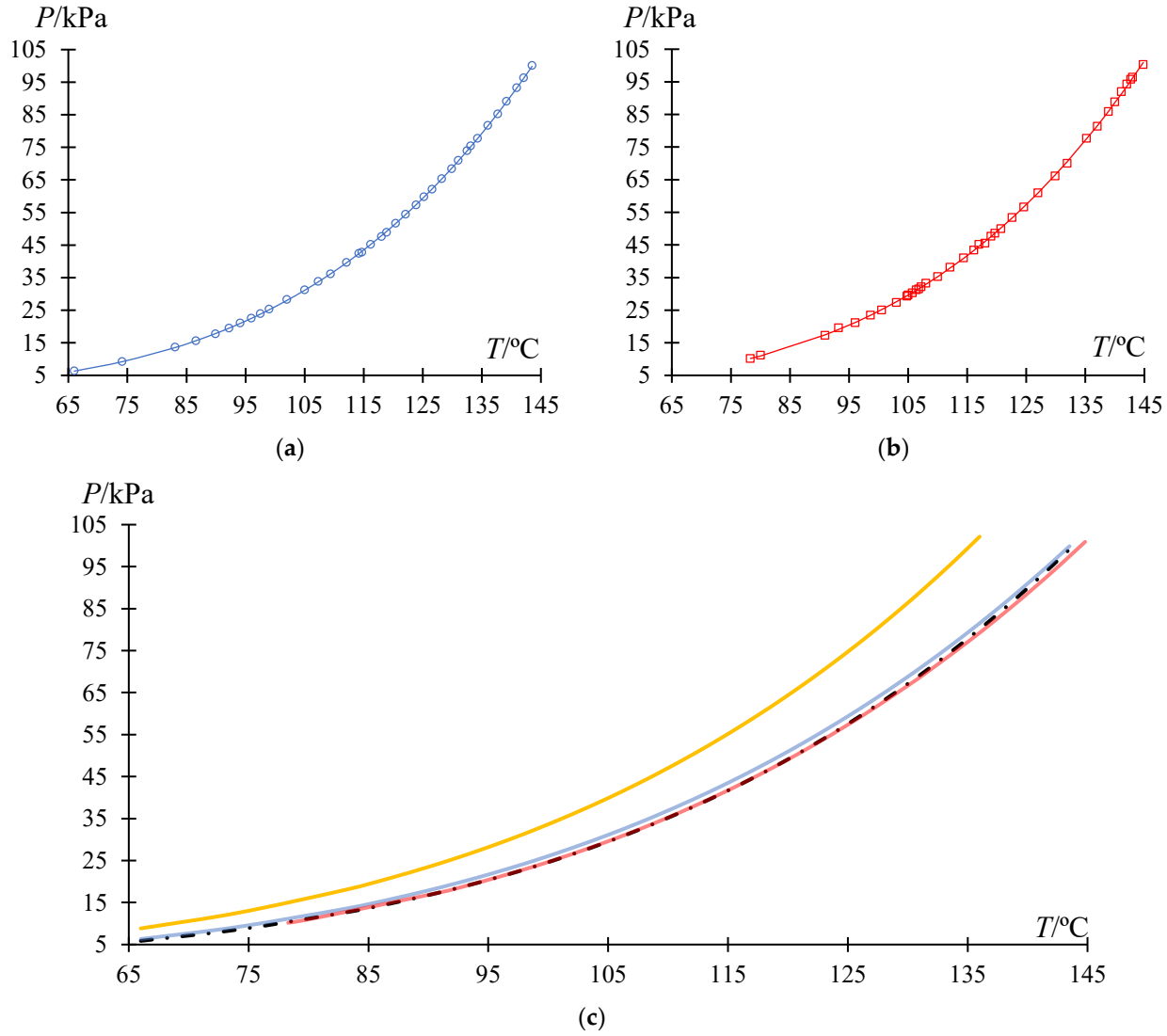

Figure 10. Dependences of the saturated vapor pressure P on temperature T. (**a**,**b**) Experimental versus calculated data; (**c**) isomeric reaction products comparison. Points represent experimental

data (Tables 5 and 6); Lines represent data calculated by the Antoine equation (trans- and cis-PFD: Table 7 data; BCH and MBCN: literature data [130]). Blue: trans-PFD; red: cis-PFD; black: BCH; yellow: MBCN.

3.6. Refractive Index

3.6.1. Pure Substances

Experimental data on the dependences of the refractive index n_D^T on temperature T of trans-PFD and cis-PFD are listed in Tables 8 and 9, respectively.

Table 8. Refractive index n_D^T versus temperature T for trans-perfluorodecalin at pressure P = 99.0 kPa [a].

T/°C	n_D	*T*/°C	n_D	*T*/°C	n_D
25.00	1.3117	37.00	1.3073	49.00	1.3027
26.00	1.3114	38.00	1.3068	50.00	1.3023
27.00	1.3110	39.00	1.3065	51.00	1.3019
28.00	1.3106	40.00	1.3061	52.00	1.3015
29.00	1.3102	41.00	1.3057	53.00	1.3011
30.00	1.3099	42.00	1.3053	54.00	1.3008
31.00	1.3095	43.00	1.3050	55.00	1.3004
32.00	1.3091	44.00	1.3046	56.00	1.3000
33.00	1.3088	45.00	1.3042	57.00	1.2996
34.00	1.3084	46.00	1.3038	58.00	1.2992
35.00	1.3080	47.00	1.3034	59.00	1.2988
36.00	1.3076	48.00	1.3031	60.00	1.2984

[a] Standard uncertainties u: $u(T)$ = 0.05 °C; $u(n_D)$ = 0.0001; $u(P)$ = 0.3 kPa.

Table 9. Refractive index n_D^T versus temperature T for cis-perfluorodecalin at pressure P = 99.2 kPa [a].

T/°C	n_D	*T*/°C	n_D	*T*/°C	n_D
15.00	1.3191	31.00	1.3131	47.00	1.3069
16.00	1.3188	32.00	1.3127	48.00	1.3065
17.00	1.3184	33.00	1.3123	49.00	1.3061
18.00	1.3180	34.00	1.3119	50.00	1.3057
19.00	1.3176	35.00	1.3115	51.00	1.3053
20.00	1.3173	36.00	1.3111	52.00	1.3050
21.00	1.3169	37.00	1.3108	53.00	1.3046
22.00	1.3165	38.00	1.3104	54.00	1.3042
23.00	1.3161	39.00	1.3100	55.00	1.3038
24.00	1.3157	40.00	1.3096	56.00	1.3034
25.00	1.3154	41.00	1.3092	57.00	1.3030
26.00	1.3150	42.00	1.3088	58.00	1.3026
27.00	1.3146	43.00	1.3085	59.00	1.3022
28.00	1.3142	44.00	1.3081	60.00	1.3018
29.00	1.3138	45.00	1.3077	-	-
30.00	1.3134	46.00	1.3073	-	-

[a] Standard uncertainties u: $u(T)$ = 0.05 °C; $u(n_D)$ = 0.0001; $u(P)$ = 0.3 kPa.

The dependences of the refractive index n_D^T for trans-PFD and cis-PFD on temperature T are described by Equation (3):

$$n_{D_i}^T = A_i^{n_D} + B_i^{n_D} \cdot T/°C \quad (3)$$

where T is temperature, and °C; $A_i^{n_D}$, and $B_i^{n_D}$represent coefficients of Equation (3). The coefficients of the equation are listed in Table 10

Table 10. Dimensionless coefficients of Equation (3)—the refractive index n_D^T dependence on temperature T for trans-perfluorodecalin and cis-perfluorodecalin for the temperature range [T_{min}, T_{max}].

Component	$A_i^{n_D}$	$B_i^{n_D}$	[T_{min}, T_{max}]/°C
trans-perfluorodecalin	1.3213	-3.80×10^{-4}	[25, 60]
cis-perfluorodecalin	1.3250	-3.85×10^{-4}	[15, 60]

The comparison of the experimental (Tables 8 and 9) and calculated (Table 10) dependences for the refractive index of trans-PFD and cis-PFD on temperature are presented in Figure 11.

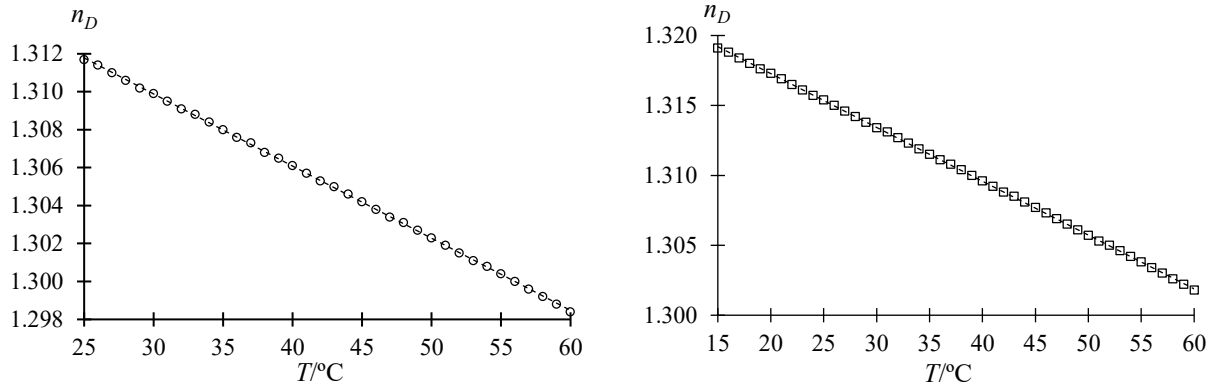

(**a**) (**b**)

Figure 11. Refractive index n_D^T versus temperature T. (**a**) trans-perfluorodecalin; (**b**) cis-perfluorodecalin. Dots: experimental data (Tables 8 and 9); line: calculated by Equation (3) (Table 10).

3.6.2. Binary Systems

Dependences of the refractive index (n_D at 15 and 25 °C) on trans-PFD–cis-PFD, BCH–trans-PFD, and BCH–cis-PFD binary system composition at atmospheric pressure are presented in Table 11 and Figure 12.

Table 11. Dependences of the refractive index n_D^T at temperature T on binary system composition x_i at atmospheric pressure P [a].

trans-PFD–cis-PFD at P = 98.2 kPa			BCH–trans-PFD at P = 100.3 kPa		BCH–cis-PFD at P = 99.4 kPa		
$x_{trans\text{-}PFD}$	n_D^{15}	n_D^{25}	x_{BCH}	n_D^{15}	x_{BCH}	n_D^{15}	n_D^{25}
0	1.3191	1.3154	0	-	0	1.3191	1.3154
0.10198	1.3187	1.3150	0.10688	1.3130	0.10343	1.3163	1.3125
0.19411	1.3184	1.3146	0.19419	1.3112	0.17164	1.3144	1.3107
0.30439	1.3180	1.3142	0.29614	1.3091	0.28538	1.3116	1.3079
0.37857	1.3178	1.3139	0.40515	1.3070	0.40622	1.3089	1.3052
0.49848	1.3173	1.3135	0.49698	1.3053	0.50224	1.3066	1.3029
0.60085	1.3169	1.3131	0.59993	1.3034	0.60547	1.3044	1.3007
0.70172	1.3167	1.3129	0.69763	1.3017	0.66844	1.3027	1.2996
0.80201	1.3162	1.3125	0.80471	1.2999	0.80202	1.3005	1.2968
0.90273	1.3159	1.3121	0.89712	1.2979	0.88860	1.2988	1.2952
1	-	1.3117	1	1.297	1	1.2970	-

[a] Standard uncertainties u: $u(T)$ = 0.05 °C, $u(n_D)$ = 0.0001, $u(P)$ = 0.3 kPa, $u(x_i)$ = 0.00006.

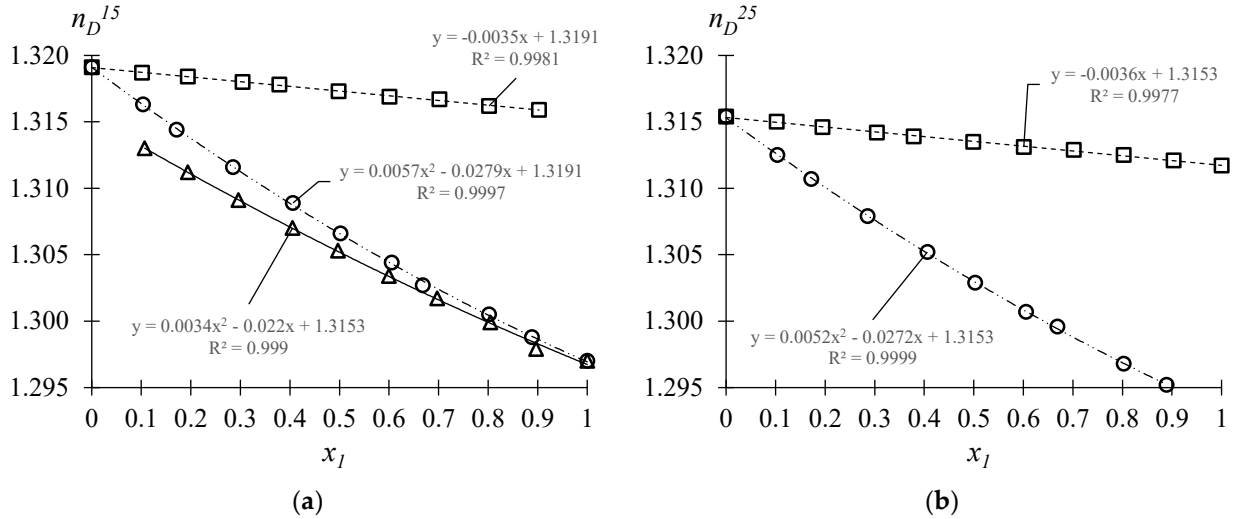

Figure 12. Dependences of the refractive index n_D^T on binary system composition x_i according to the Table 11 data. (**a**) 15 °C; (**b**) 25 °C. Square trans-PFD (1)–cis-PFD (2); circle BCH (1)–cis-PFD (2); triangular BCH (1)–trans-PFD (2).

The equation for the dependence of the refractive index on the compositions of the trans-PFD–cis-PFD, BCH–trans-PFD, and BCH–cis-PFD binary systems was generated based on the data shown in Figure 12; the coefficients for Equation (4) are listed in Table 12:

$$n_D = a_0^{n_D} + a_1^{n_D} x_1 + a_2^{n_D} x_1^2 \quad (4)$$

where x_1 is the composition, mole fraction; $a_0^{n_D}$, $a_1^{n_D}$, and $a_2^{n_D}$ are coefficients of Equation (4).

Table 12. Dimensionless coefficients of Equation (4)—the refractive index n_D^T dependence on binary systems composition x_i at temperature T.

System	trans-PFD (1)–cis-PFD (2)		BCH (1)–trans-PFD (2)	BCH (1)–cis-PFD (2)	
T/°C	15	25	15	15	25
$a_0^{n_D}$	1.3191	1.3153	1.3153	1.3191	1.3153
$a_1^{n_D}$	−0.0035	−0.0036	−0.0220	−0.0279	−0.0272
$a_2^{n_D}$	0	0	0.0034	0.0057	0.0052

3.6.3. Ternary System

Dependence of the refractive index (n_D at 15 and 25 °C) on the BCH–trans-PFD–cis-PFD ternary system composition at atmospheric pressure is presented in Table 13 and Figure 13.

Table 13. Dependences of the refractive index n_D^T at temperature T on BCH (1)–trans-PFD (2)–cis-PFD (3) ternary system composition x_i at pressure P = 99.1 kPa [a].

x_1	x_2	x_3	n_D^{15}	n_D^{25}
0.57402	0.21988	0.20610	1.3046	1.3003
0.17937	0.63244	0.18819	1.3121	1.3085
0.17479	0.19519	0.63002	1.3137	1.3099
0.18870	0.39863	0.41267	1.3128	1.3091
0.37885	0.22255	0.39860	1.3087	1.3050
0.36974	0.40875	0.22151	1.3083	1.3046

[a] Standard uncertainties u: $u(T)$ = 0.05 °C, $u(n_D)$ = 0.0001, $u(P)$ = 0.3 kPa, $u(x_i)$ = 0.00005.

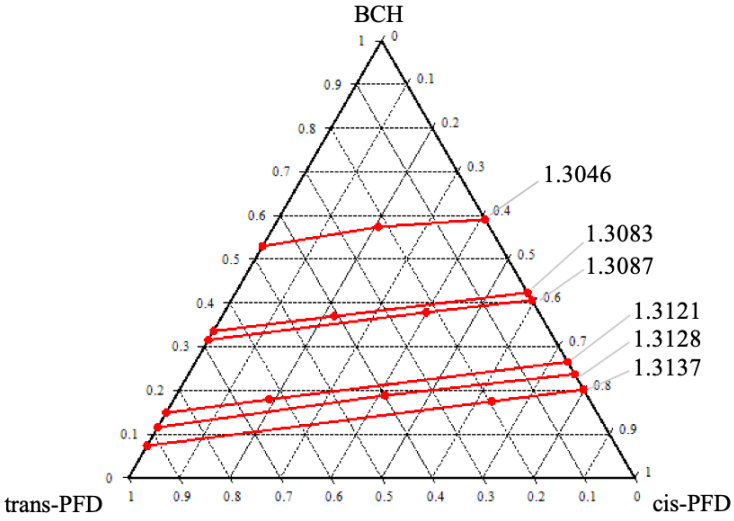

Figure 13. Dependence of the isoline of refractive index on ternary system composition according to the data from Tables 12 and 13 at 15 °C.

3.7. Density and Liquid Molar Volume

3.7.1. Pure Substances

Experimental data on the dependences of the density ρ_i and liquid molar volume V_{M_i} on the temperature of trans-PFD and cis-PFD are presented in Tables 14 and 15, respectivcely.

Table 14. Density ρ and liquid molar volume V_M versus temperature T for trans-perfluorodecalin at pressure P = 99.0 kPa [a].

T/°C	*ρ*/g·cm⁻³	*V*M/cm³·mol⁻¹	*T*/°C	*ρ*/g·cm⁻³	*V*M/cm³·mol⁻¹	*T*/°C	*ρ*/g·cm⁻³	*V*M/cm³·mol⁻¹
25.00	1.92344	240.236	37.00	1.89637	243.666	49.00	1.86915	247.214
26.00	1.92116	240.521	38.00	1.89411	243.956	50.00	1.86687	247.516
27.00	1.91890	240.805	39.00	1.89186	244.246	51.00	1.86458	247.820
28.00	1.91663	241.090	40.00	1.88960	244.539	52.00	1.86230	248.123
29.00	1.91438	241.373	41.00	1.88734	244.831	53.00	1.86002	248.427
30.00	1.91213	241.657	42.00	1.88507	245.126	54.00	1.85771	248.736
31.00	1.90987	241.943	43.00	1.88280	245.422	55.00	1.85542	249.043
32.00	1.90763	242.227	44.00	1.88053	245.718	56.00	1.85312	249.352
33.00	1.90537	242.515	45.00	1.87826	246.015	57.00	1.85083	249.661
34.00	1.90312	242.801	46.00	1.87599	246.313	58.00	1.84850	249.976
35.00	1.90087	243.089	47.00	1.87371	246.612	59.00	1.84620	250.287
36.00	1.89862	243.377	48.00	1.87143	246.913	60.00	1.84389	250.601

[a] Standard uncertainties u: $u(T)$ = 0.05 °C; $u(\rho)$ = 0.0001 g·cm⁻³; $u(P)$ = 0.3 kPa.

Table 15. Density ρ and liquid molar volume V_M versus temperature T for cis-perfluorodecalin at pressure P = 99.2 kPa [a].

T/°C	*ρ*/g·cm⁻³	*V*M/cm³·mol⁻¹	*T*/°C	*ρ*/g·cm⁻³	*V*M/cm³·mol⁻¹	*T*/°C	*ρ*/g·cm⁻³	*V*M/cm³·mol⁻¹
15.00	1.96878	234.704	31.00	1.93225	239.141	47.00	1.89598	243.716
16.00	1.96653	234.972	32.00	1.93025	239.389	48.00	1.89354	244.030
17.00	1.96427	235.243	33.00	1.92797	239.672	49.00	1.89133	244.315
18.00	1.96201	235.514	34.00	1.92569	239.956	50.00	1.88908	244.606
19.00	1.95973	235.788	35.00	1.92341	240.240	51.00	1.88674	244.909
20.00	1.95746	236.061	36.00	1.92113	240.525	52.00	1.88442	245.211

21.00	1.95520	236.334	37.00	1.91885	240.811	53.00	1.88209	245.514
22.00	1.95293	236.609	38.00	1.91656	241.099	54.00	1.87975	245.820
23.00	1.95066	236.884	39.00	1.91427	241.387	55.00	1.87743	246.124
24.00	1.94840	237.159	40.00	1.91198	241.676	56.00	1.87510	246.430
25.00	1.94613	237.435	41.00	1.90968	241.967	57.00	1.87276	246.737
26.00	1.94387	237.711	42.00	1.90738	242.259	58.00	1.87043	247.045
27.00	1.94160	237.989	43.00	1.90509	242.550	59.00	1.86810	247.353
28.00	1.93933	238.268	44.00	1.90278	242.845	60.00	1.86576	247.663
29.00	1.93707	238.546	45.00	1.90064	243.118	-	-	-
30.00	1.93480	238.826	46.00	1.89829	243.419	-	-	-

[a] Standard uncertainties u: $u(T)$ = 0.05 °C; $u(\rho)$ = 0.0001 g·cm^{-3}; $u(P)$ = 0.3 kPa.

Liquid molar volume $V_{M\,i}$ presented in Tables 14 and 15 was calculated according to Equation (5):

$$V_{M\,i} = \frac{M_i}{\rho_i} \quad (5)$$

where M_i is molecular weight, g·mol^{-1}; ρ_i is density, g·cm^{-3}.

The dependences of the density ρ_i of trans-PFD and cis-PFD on temperature T are described by Equation (6):

$$\rho_i(\mathrm{g \cdot cm^{-3}}) = A_i^{\rho} + B_i^{\rho} \cdot T/°C \quad (6)$$

where T is temperature, °C; A_i^{ρ} and B_i^{ρ} are coefficients of Equation (6); the coefficients are listed in Table 16

Table 16. Coefficients of Equation (6)—the density (ρ) dependence on temperature (T) for trans-perfluorodecalin and cis-perfluorodecalin.

Component	A_i^{ρ}	B_i^{ρ}	$[T_{min}, T_{max}]$/°C
Trans-perfluorodecalin	1.98029	−0.00227	[25, 60]
Cis-perfluorodecalin	2.00330	−0.00229	[15, 60]

The comparison of the calculated (Table 16) and experimental (Tables 14 and 15) dependences for the density and liquid molar volume of trans-PFD and cis-PFD on temperature are presented in Figure 14.

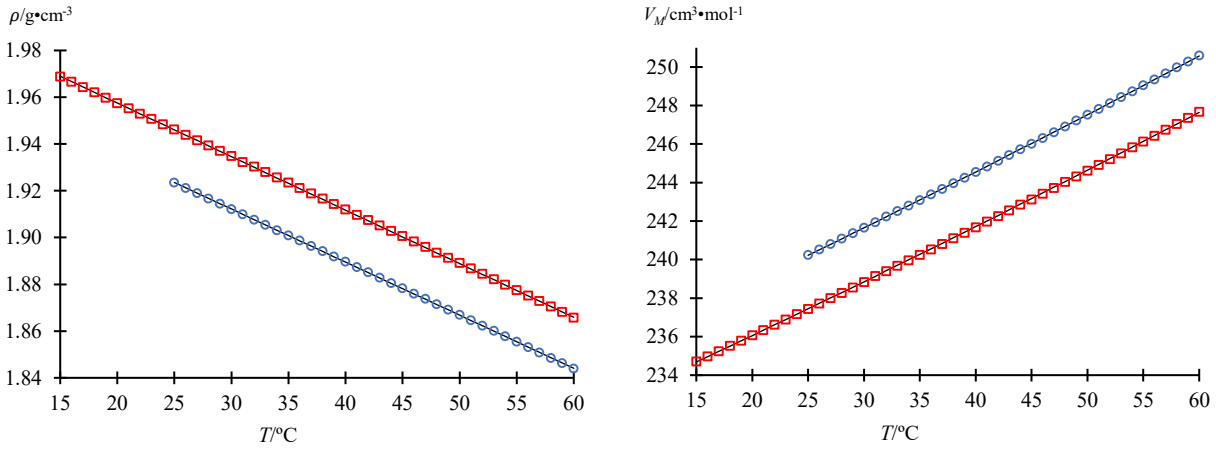

(**a**) (**b**)

Figure 14. Experimental values of density ρ (**a**) and liquid molar volume V_M (**b**) versus temperature T. blue dots: trans-perfluorodecalin (Table 14), red dots: cis-perfluorodecalin (Table 15), lines: data calculated by Equations (5) and (6) (Table 16).

3.7.2. Binary Systems

Dependences of density on the composition of BCH–cis-PFD, BCH–trans-PFD, and trans-PFD–cis-PFD systems at different temperatures are presented in Tables 17–19, respectively.

Table 17. Dependences of density ρ on perfluoro(butylcyclohexane) (1)–cis-perfluorodecalin (2) system composition x_i at temperature T and pressure P [a].

		***T*/°C**									
x_1	***P*/kPa**	**15**	**20**	**25**	**30**	**35**	**40**	**45**	**50**	**55**	**60**
		ρ/g·cm^{-3}									
0	99.2	1.96878	1.95746	1.94613	1.93480	1.92341	1.91198	1.90048	1.88908	1.87743	1.86576
0.10343		1.95773	1.94661	1.93538	1.92409	1.91274	1.90134	1.88990	1.87837	1.86681	1.85514
0.17164	98.8	1.95040	1.93938	1.92823	1.91699	1.90568	1.89431	1.88287	1.87133	1.85977	1.84813
0.28538		1.93986	1.92883	1.91769	1.90648	1.89518	1.88382	1.87239	1.86088	1.84931	1.83769
0.31744	100.5	1.93729	1.92620	1.91502	1.90376	1.89245	1.88103	1.86963	1.85817	1.84662	1.83500
0.35826		1.93361	1.92262	1.91148	1.90026	1.88896	1.87761	1.86616	1.85466	1.84311	1.83149
0.37933	98.8	1.93190	1.92084	1.90966	1.89842	1.88711	1.87577	1.86434	1.85285	1.84132	1.82971
0.39919		1.92998	1.91897	1.90783	1.89661	1.88532	1.87394	1.86252	1.85100	1.83945	1.82783
0.44022	100.5	1.92669	1.91568	1.90455	1.89334	1.88204	1.87067	1.85925	1.84772	1.83616	1.82452
0.50224	98.9	1.92200	1.91097	1.89981	1.88859	1.87728	1.86590	1.85445	1.84290	1.83134	1.81967
0.60547		1.91379	1.90281	1.89167	1.88044	1.86912	1.85772	1.84626	1.83471	1.82309	1.81141
0.69350		1.90737	1.89625	1.88502	1.87373	1.86236	1.85095	1.83944	1.82786	1.81625	1.80453
0.80202	100.3	1.89986	1.88879	1.87760	1.86631	1.85493	1.84345	1.83192	1.82027	1.80859	1.79682
0.88860		1.89420	1.88309	1.87186	1.86052	1.84911	1.83760	1.82603	1.81436	1.80264	1.79081
1	99.3	1.88829	1.87697	1.86563	1.85429	1.84283	1.83130	1.81969	1.80795	1.79625	1.78436

[a] Standard uncertainties u: $u(T)$ = 0.05 °C; $u(x_i)$ = 0.00005; $u(\rho)$ = 0.0001 g·cm^{-3}; $u(P)$ = 0.3 kPa.

Table 18. Dependences of the density ρ on perfluoro(butylcyclohexane) (1)–trans-perfluorodecalin (2) system composition x_i at temperature T and pressure P [a].

		***T*/°C**							
x_1	***P*/kPa**	**25**	**30**	**35**	**40**	**45**	**50**	**55**	**60**
		ρ/g·cm^{-3}							
0	98.1	1.92344	1.91213	1.90087	1.88960	1.87826	1.86687	1.85542	1.84389
0.10688		1.91545	1.90436	1.89319	1.88195	1.87063	1.85923	1.84778	1.83623
0.19419	100.7	1.90908	1.89804	1.88689	1.87565	1.86434	1.85294	1.84149	1.82996
0.29614		1.90250	1.89142	1.88025	1.86900	1.85767	1.84624	1.83478	1.82322
0.40516		1.89601	1.88487	1.87363	1.86233	1.85096	1.83953	1.82801	1.81643
0.49698	99.3	1.89052	1.87939	1.86815	1.85684	1.84545	1.83396	1.82240	1.81078
0.59993		1.88470	1.87354	1.86227	1.85091	1.83947	1.82794	1.81635	1.80468
0.69763		1.87961	1.86836	1.85703	1.84562	1.83415	1.82258	1.81093	1.79920
0.80471	99.7	1.87398	1.86272	1.85135	1.83990	1.82837	1.81675	1.80507	1.79330
0.89712		1.86994	1.85859	1.84715	1.83560	1.82404	1.81237	1.80064	1.78882
1	99.3	1.86563	1.85429	1.84283	1.83130	1.81969	1.80795	1.79625	1.78436

[a] Standard uncertainties u: $u(T)$ = 0.05 °C; $u(x_i)$ = 0.00006; $u(\rho)$ = 0.0001 g·cm^{-3}; $u(P)$ = 0.3 kPa.

Table 19. Dependences of the density ρ on trans-perfluorodecalin (1)–cis-perfluorodecalin (2) system composition x_i at temperature T and pressure P [a].

x_1	P/kPa	T/°C							
		25	30	35	40	45	50	55	60
		ρ/g·cm^{-3}							
0	99.2	1.94613	1.93480	1.92341	1.91198	1.90079	1.88908	1.87743	1.86576
0.10198		1.94389	1.93263	1.92128	1.90985	1.89839	1.88684	1.87527	1.86360
0.19411	100.9	1.94178	1.93058	1.91926	1.90787	1.89640	1.88487	1.87330	1.86165
0.30439		1.93933	1.92811	1.91681	1.90544	1.89397	1.88244	1.87085	1.85919
0.41417	100.0	1.93671	1.92547	1.91416	1.90279	1.89136	1.87988	1.86832	1.85670
0.49848	100.8	1.93455	1.92338	1.91210	1.90076	1.88933	1.87785	1.86631	1.85470
0.60085		1.93220	1.92104	1.90978	1.89845	1.88704	1.87557	1.86404	1.85246
0.70172	99.7	1.92985	1.91870	1.90745	1.89617	1.88479	1.87335	1.86184	1.85029
0.80539	100.1	1.92740	1.91631	1.90510	1.89382	1.88247	1.87106	1.85956	1.84799
0.90273	99.7	1.92528	1.91420	1.90300	1.89173	1.88039	1.86895	1.85746	1.84592
1	98.1	1.92344	1.91213	1.90087	1.88960	1.87826	1.86687	1.85542	1.84389

[a] Standard uncertainties u: $u(T)$ = 0.05 °C; $u(x_i)$ = 0.00006; $u(\rho)$ = 0.0001 g·cm^{-3}; $u(P)$ = 0.3 kPa.

The liquid molar volume V_M of the BCH–cis-PFD, BCH–trans-PFD, and trans-PFD–cis-PFD systems was calculated according to Equation (7) and is presented in Tables 20–22, respectively. Additionally, the excess molar volume V^E of the BCH–cis-PFD, BCH–trans-PFD, and trans-PFD–cis-PFD systems was calculated according to Equation (8) and is presented in Tables 23–25, respectively. The V_M and V^E data (Tables 20–25) provide the maximum standard uncertainties u of the values; standard uncertainties u for each experimental point are provided in Appendix A (Tables A1–A6, respectively).

$$V_M = \frac{\sum_{i=1}^{i} M_i x_i}{\rho_{mixture}} \quad (7)$$

$$V^E = \frac{x_i M_i + x_j M_j}{\rho_{mixture}} - \left(x_i \frac{M_i}{\rho_i} + x_j \frac{M_j}{\rho_j} \right) \quad (8)$$

where M_i is the molecular weight, g·mol^{-1}; $\rho_{mixture}$ is the mixture density at composition x_i, g·cm^{-3}.

Table 20. Dependences of the liquid molar volume V_M on perfluoro(butylcyclohexane) (1)–cis-perfluorodecalin (2) system composition x_i at temperature T [a].

x_1	T/°C									
	15	20	25	30	35	40	45	50	55	60
	V_M/cm^{-3}·mol^{-1}									
0	234.704	236.061	237.435	238.826	240.240	241.676	243.139	244.606	246.124	247.663
0.10343	238.036	239.395	240.784	242.197	243.634	245.095	246.579	248.092	249.629	251.199
0.17164	240.259	241.624	243.021	244.446	245.897	247.373	248.876	250.410	251.967	253.554
0.28538	243.792	245.186	246.610	248.060	249.539	251.044	252.576	254.139	255.729	257.346
0.31744	244.744	246.153	247.590	249.054	250.543	252.064	253.601	255.165	256.761	258.387
0.35826	246.012	247.418	248.860	250.329	251.827	253.349	254.903	256.484	258.091	259.729
0.37933	246.644	248.064	249.516	250.993	252.498	254.024	255.581	257.166	258.777	260.419
0.39919	247.280	248.699	250.151	251.631	253.138	254.675	256.236	257.831	259.450	261.099
0.44022	248.511	249.939	251.400	252.889	254.407	255.953	257.525	259.132	260.764	262.427
0.50224	250.343	251.788	253.267	254.772	256.307	257.870	259.462	261.089	262.737	264.422
0.60547	253.467	254.929	256.430	257.962	259.524	261.117	262.738	264.392	266.077	267.792

0.69350	256.073	257.575	259.109	260.670	262.262	263.879	265.530	267.212	268.920	270.667
0.80202	259.255	260.775	262.329	263.916	265.535	267.189	268.870	270.591	272.339	274.122
0.88860	261.766	263.311	264.890	266.505	268.149	269.829	271.539	273.285	275.062	276.879
1	264.827	266.424	268.044	269.683	271.360	273.068	274.811	276.595	278.397	280.252

[a] Standard uncertainties u: $u(T)$ = 0.05 °C; $u(x_i)$ = 0.00005; $u(V_M)$ = 0.025 cm^{-3}·mol^{-1}.

Table 21. Dependences of the liquid molar volume V_M on perfluoro(butylcyclohexane) (1)–trans-perfluorodecalin (2) system composition x_i at temperature T [a].

	T/°C							
x_1	**25**	**30**	**35**	**40**	**45**	**50**	**55**	**60**
	V_M/cm^{-3}·mol^{-1}							
0	240.236	241.657	243.089	244.539	246.015	247.516	249.043	250.601
0.10688	243.358	244.775	246.220	247.690	249.189	250.717	252.270	253.857
0.19419	245.908	247.338	248.799	250.290	251.809	253.358	254.933	256.540
0.29614	248.794	250.251	251.738	253.253	254.798	256.375	257.977	259.612
0.40516	251.830	253.318	254.838	256.384	257.959	259.562	261.198	262.863
0.49698	254.406	255.913	257.453	259.021	260.620	262.252	263.916	265.609
0.59993	257.267	258.800	260.366	261.964	263.593	265.256	266.948	268.674
0.69763	259.938	261.504	263.099	264.726	266.381	268.072	269.797	271.556
0.80471	262.890	264.479	266.104	267.760	269.448	271.172	272.926	274.718
0.89712	265.336	266.956	268.609	270.299	272.012	273.764	275.547	277.368
1	268.044	269.683	271.360	273.068	274.811	276.595	278.397	280.252

[a] Standard uncertainties u: $u(T)$ = 0.05 °C; $u(x_i)$ = 0.00006; $u(V_M)$ = 0.028 cm^{-3}·mol^{-1}.

Table 22. Dependences of the liquid molar volume V_M on trans-perfluorodecalin (1)–cis-perfluorodecalin (2) system composition x_i at temperature T [a].

	T/°C							
x_1	**25**	**30**	**35**	**40**	**45**	**50**	**55**	**60**
	V_M/cm^{-3}·mol^{-1}							
0	237.435	238.826	240.240	241.676	243.099	244.606	246.124	247.663
0.10198	237.709	239.094	240.506	241.946	243.406	244.896	246.407	247.950
0.19411	237.967	239.348	240.759	242.197	243.662	245.152	246.666	248.210
0.30439	238.268	239.654	241.067	242.506	243.974	245.469	246.989	248.538
0.41417	238.590	239.983	241.401	242.843	244.311	245.803	247.324	248.872
0.49848	238.857	240.244	241.661	243.103	244.573	246.069	247.590	249.140
0.60085	239.147	240.536	241.955	243.399	244.870	246.368	247.892	249.441
0.70172	239.438	240.830	242.250	243.691	245.163	246.660	248.185	249.734
0.80539	239.743	241.130	242.549	243.994	245.465	246.962	248.489	250.045
0.90273	240.007	241.396	242.817	244.263	245.736	247.240	248.770	250.325
1	240.236	241.657	243.089	244.539	246.015	247.516	249.043	250.601

[a] Standard uncertainties u: $u(T)$ = 0.05 °C; $u(x_i)$ = 0.00006; $u(V_M)$ = 0.014 cm^{-3}·mol^{-1}.

Table 23. Dependences of the excess molar volume V^E on perfluoro(butylcyclohexane) (1)–cis-perfluorodecalin (2) system composition x_i at temperature T [a].

	T/°C									
x_1	**15**	**20**	**25**	**30**	**35**	**40**	**45**	**50**	**55**	**60**
	V^E/cm^{-3}·mol^{-1}									
0	0	0	0	0	0	0	0	0	0	0
0.10343	0.216	0.194	0.183	0.179	0.175	0.172	0.164	0.177	0.167	0.165
0.17164	0.385	0.351	0.332	0.324	0.316	0.309	0.301	0.313	0.304	0.297
0.28538	0.491	0.460	0.440	0.428	0.418	0.409	0.398	0.404	0.395	0.383

0.31744	0.478	0.454	0.438	0.433	0.424	0.423	0.408	0.404	0.392	0.379
0.35826	0.516	0.479	0.459	0.448	0.438	0.427	0.417	0.418	0.405	0.391
0.37933	0.513	0.485	0.470	0.462	0.453	0.440	0.428	0.426	0.411	0.394
0.39919	0.551	0.517	0.497	0.487	0.475	0.468	0.454	0.455	0.443	0.427
0.44022	0.546	0.512	0.490	0.479	0.467	0.458	0.443	0.444	0.433	0.418
0.50224	0.510	0.477	0.459	0.448	0.437	0.428	0.416	0.417	0.404	0.392
0.60547	0.524	0.484	0.462	0.453	0.442	0.434	0.423	0.418	0.413	0.397
0.69350	0.479	0.457	0.447	0.445	0.440	0.433	0.426	0.422	0.415	0.404
0.80202	0.392	0.362	0.345	0.342	0.336	0.336	0.329	0.329	0.331	0.322
0.88860	0.295	0.269	0.256	0.259	0.256	0.258	0.256	0.254	0.260	0.257
1	0	0	0	0	0	0	0	0	0	0

[a] Standard uncertainties u: $u(T)$ = 0.05 °C; $u(x_i)$ = 0.00005; $u(V^E)$ = 0.034 cm^{-3}·mol^{-1}.

Table 24. Dependences of the excess molar volume V^E on perfluoro(butylcyclohexane) (1)–trans-perfluorodecalin (2) system composition x_i at temperature T [a].

	T/°C							
x_1	**25**	**30**	**35**	**40**	**45**	**50**	**55**	**60**
	V^E/cm^{-3}·mol^{-1}							
0	0	0	0	0	0	0	0	0
0.10688	0.150	0.123	0.109	0.102	0.096	0.093	0.090	0.087
0.19419	0.272	0.239	0.220	0.211	0.202	0.195	0.190	0.181
0.29614	0.323	0.294	0.277	0.265	0.255	0.248	0.241	0.230
0.40516	0.327	0.306	0.295	0.286	0.277	0.264	0.262	0.249
0.49698	0.350	0.328	0.314	0.304	0.294	0.284	0.285	0.272
0.59993	0.348	0.329	0.316	0.310	0.302	0.295	0.295	0.284
0.69763	0.302	0.295	0.287	0.284	0.277	0.270	0.276	0.270
0.80471	0.277	0.269	0.265	0.263	0.261	0.256	0.262	0.257
0.89712	0.153	0.156	0.158	0.166	0.164	0.161	0.170	0.166
1	0	0	0	0	0	0	0	0

[a] Standard uncertainties u: $u(T)$ = 0.05 °C; $u(x_i)$ = 0.00006; $u(V^E)$ = 0.038 cm^{-3}·mol^{-1}.

Table 25. Dependences of the excess molar volume V^E on trans-perfluorodecalin (1)–cis-perfluorodecalin (2) system composition x_i at temperature T [a].

	T/°C							
x_1	**25**	**30**	**35**	**40**	**45**	**50**	**55**	**60**
	V^E/cm^{-3}·mol^{-1}							
0	0	0	0	0	0	0	0	0
0.10198	−0.012	−0.021	−0.025	−0.022	0.010	−0.007	−0.015	−0.013
0.19411	−0.012	−0.028	−0.034	−0.035	−0.003	−0.019	−0.025	−0.023
0.30439	−0.020	−0.034	−0.040	−0.041	−0.013	−0.023	−0.024	−0.019
0.41417	−0.005	−0.016	−0.019	−0.019	0.004	−0.008	−0.009	−0.008
0.49848	0.026	0.007	0.001	0	0.020	0.012	0.011	0.012
0.60085	0.029	0.009	0.003	0.003	0.019	0.014	0.014	0.013
0.70172	0.037	0.017	0.011	0.006	0.018	0.012	0.013	0.009
0.80539	0.052	0.024	0.014	0.012	0.017	0.012	0.014	0.016
0.90273	0.043	0.014	0.005	0.002	0.005	0.007	0.011	0.010
1	0	0	0	0	0	0	0	0

[a] Standard uncertainties u: $u(T)$ = 0.05 °C; $u(x_i)$ = 0.00006; $u(V^E)$ = 0.025 cm^{-3}·mol^{-1}.

The excess molar volume data (Tables 23–25) were correlated with the Redlich-Kister [138] Equation (9a). The Redlich-Kister parameters are presented in Tables 26–28. The

standard deviation σ between experimental (Tables 23–25) and calculated by Equation (9a) (Tables 26–28, accordingly) data were calculated according to Equation (9b) [139].

$$V^E = x_1 x_2 \sum_{i=0}^{i} a_i (x_1 - x_2)^i \quad (9a)$$

$$\sigma(V^E) = \sqrt{\frac{\sum \left(V^E_{exp} - V^E_{calc}\right)^2}{d - \tilde{n}}} \quad (9b)$$

where a_i represents the Redlich-Kister parameters; d is the number of compositions studied; ñ represents the number of terms used in the regression.

Table 26. Redlich-Kister regression results (according to the Equation (9a,b)) for the excess molar volumes V^E at temperature T of perfluoro(butylcyclohexane) (1)–cis-perfluorodecalin (2) system calculated from Table 23 data.

T/°C	a_3	a_2	a_1	a_0	$\sigma(V^E)$/cm³·mol⁻¹
15	1.104964	0.978578	−0.344386	2.129725	0.021
20	1.062583	0.771174	−0.326034	2.008629	0.019
25	1.006494	0.675298	−0.295903	1.938418	0.018
30	1.054220	0.720329	−0.277812	1.898207	0.018
35	1.042090	0.725251	−0.260297	1.856007	0.018
40	1.097235	0.774554	−0.255016	1.817599	0.018
45	1.136660	0.774213	−0.243640	1.767653	0.018
50	0.985911	0.886383	−0.249339	1.755389	0.018
55	1.124080	0.934376	−0.232019	1.709023	0.019
60	1.098612	0.985980	−0.221599	1.644507	0.018

Table 27. Redlich-Kister regression results (according to Equation (9a,b)) for the excess molar volumes V^E at temperature T of perfluoro(butylcyclohexane) (1)–trans-perfluorodecalin (2) system calculated from Table 24 data.

T/°C	a_4	a_3	a_2	a_1	a_0	$\sigma(V^E)$/cm³·mol⁻¹
25	−1.954153	0.190090	1.674633	−0.058943	1.343112	0.018
30	−1.845871	0.425479	1.529335	−0.003537	1.264095	0.014
35	−1.727888	0.544906	1.430764	0.021673	1.215389	0.013
40	−1.492634	0.699904	1.345204	0.020418	1.183338	0.012
45	−1.502029	0.689572	1.344187	0.056314	1.146885	0.012
50	−1.512829	0.657437	1.354771	0.072389	1.106092	0.012
55	−1.334099	0.710743	1.304439	0.124689	1.104640	0.012
60	−1.295411	0.631341	1.298648	0.165574	1.060024	0.010

Table 28. Redlich-Kister regression results (according to Equation (9a,b)) for the excess molar volumes V^E at temperature T of trans-perfluorodecalin (1)–cis-perfluorodecalin (2) system calculated from Table 25 data.

T/°C	a_1	a_0	$\sigma(V^E)$/cm³·mol⁻¹
25	0.363697	0.099868	0.011
30	0.259612	−0.019726	0.006
35	0.232529	−0.060487	0.008
40	0.205715	−0.066386	0.009
45	0.093063	0.034057	0.010
50	0.135899	−0.002282	0.008
55	0.194350	−0.010696	0.007
60	0.175727	−0.005742	0.006

The dependences for the excess molar volume of the BCH–cis-PFD, BCH–trans-PFD and trans-PFD–cis-PFD systems on composition and temperature were correlated using Equation (10a,b); the parameters were calculated from Tables 26–28 data and are listed in Tables 29–31. The standard deviation σ (Equation (9b)) between experimental (Tables 23–25) and calculated by Equation (10a,b) (Tables 29–31) data for each temperature are given in Appendix A (Tables A7–A9, respectively).

$$V^E = x_1 x_2 \sum_{i=0}^{i} a_i (x_1 - x_2)^i \quad (10a)$$

$$a_i = \sum_{j=0}^{j} b_j T^j \quad (10b)$$

where a_i is the temperature-depended Redlich-Kister parameters; x is the composition of the binary system; b_j represents the parameters of Equation (10b); T is the temperature, °C.

Table 29. Redlich-Kister regression results (according to Equation (10a,b)) for the excess molar volumes V^E of perfluoro(butylcyclohexane) (1)–cis-perfluorodecalin (2) system calculated from Table 26 data [a].

a_i	b_j		
	b_2	b_1	b_0
a_3	0.000072	−0.004674	1.131143
a_2	0.000478	−0.032840	1.283535
a_1	−0.000052	0.006427	−0.428262
a_0	0.000105	−0.017362	2.333832

[a] $\sigma(V^E)$ = 0.017 cm³·mol⁻¹.

Table 30. Redlich-Kister regression results (according to Equation (10a,b)) for the excess molar volumes V^E of perfluoro(butylcyclohexane) (1)–trans-perfluorodecalin (2) system calculated from Table 27 data [a].

a_i	b_j		
	b_2	b_1	b_0
a_4	−0.000293	0.043508	−2.864105
a_3	−0.000873	0.085766	−1.384216
a_2	0.000439	−0.046791	2.548607
a_1	0.000048	0.001634	−0.112666
a_0	0.000137	−0.019123	1.725379

[a] $\sigma(V^E)$ = 0.010 cm³·mol⁻¹.

Table 31. Redlich-Kister regression results (according to Equation (10a,b)) for the excess molar volumes V^E of trans-perfluorodecalin (1)–cis-perfluorodecalin (2) system calculated from Table 28 data [a].

a_i	b_j		
	b_2	b_1	b_0
a_1	0.000388	−0.037870	1.064833
a_0	0.000233	−0.020799	0.428681

[a] $\sigma(V^E)$ = 0.010 cm³·mol⁻¹.

Comparisons of the experimental (Tables 23–25) and calculated by Equation (9a) (Tables 26–28) or Equation (10) (Tables 29–31) data for the BCH–cis-PFD, BCH–trans-PFD, and trans-PFD–cis-PFD systems are presented in Figures 15–17, respectively.

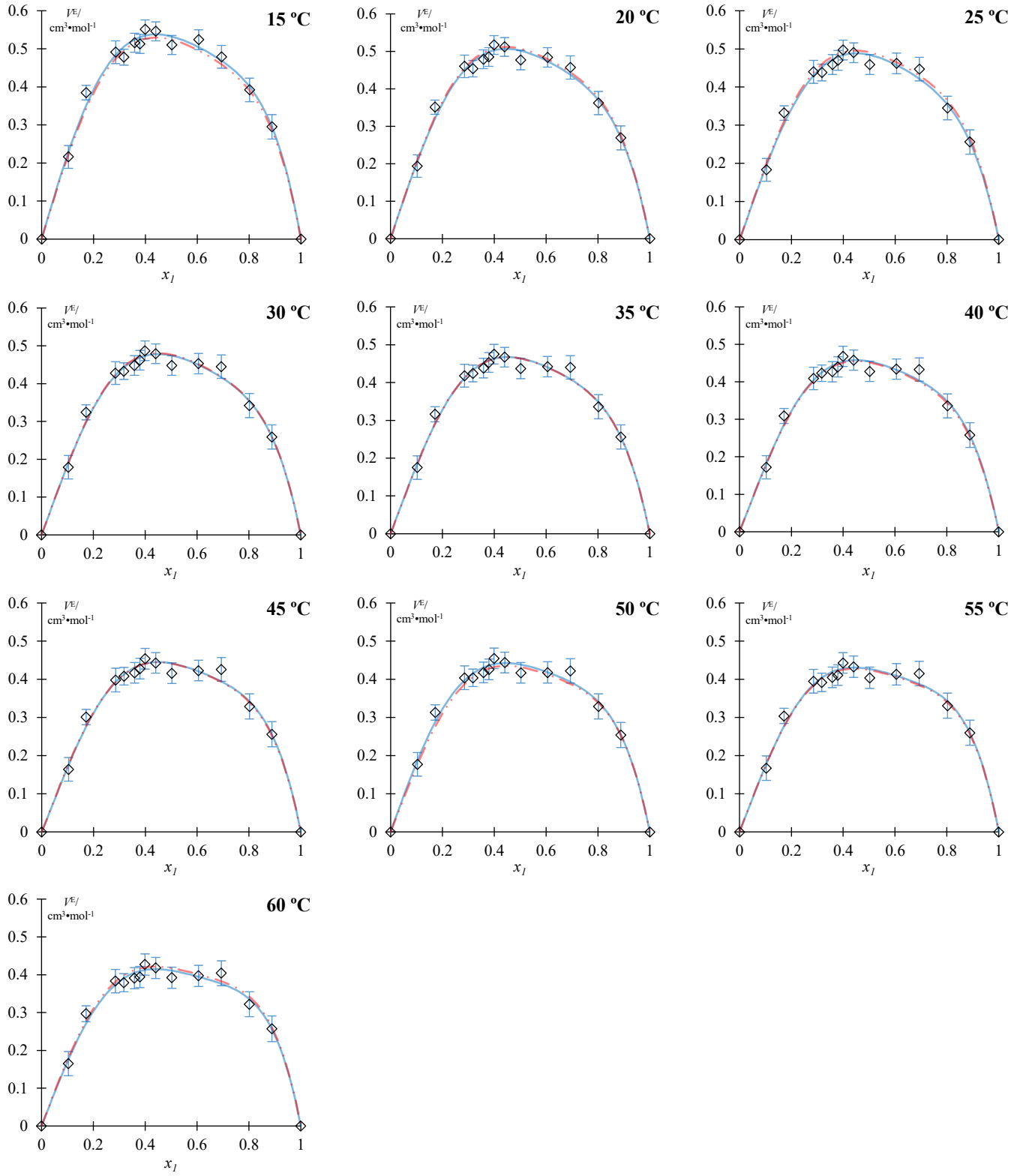

Figure 15. Dependences of the excess molar volume V^E versus concentration x_i in the perfluoro(butylcyclohexane) (1)–cis-perfluorodecalin (2) system at temperature T. Points: experimental data according to Table 23; lines: calculated data according to the Redlich-Kister equation; red: Equation (9a)—Table 26; blue: Equation (10a,b)—Table 29.

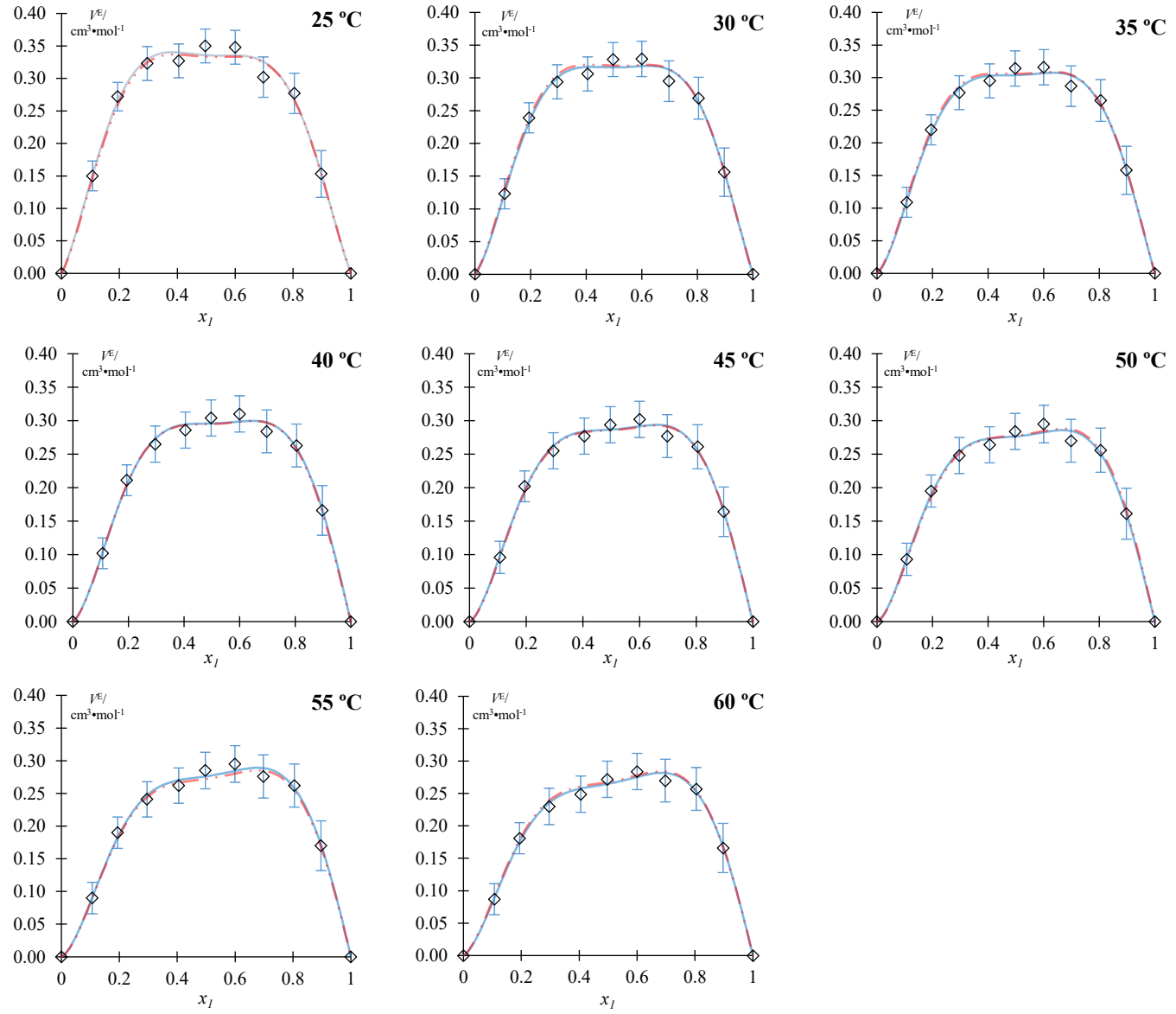

Figure 16. Dependences of the excess molar volume V^E versus concentration x_i in the perfluoro(butylcyclohexane) (1)–trans-perfluorodecalin (2) system at temperature T. Points: experimental data according to Table 24; lines: calculated data according to the Redlich-Kister equation; red: Equation (9a)—Table 27; blue: Equation (10a,b)—Table 30.

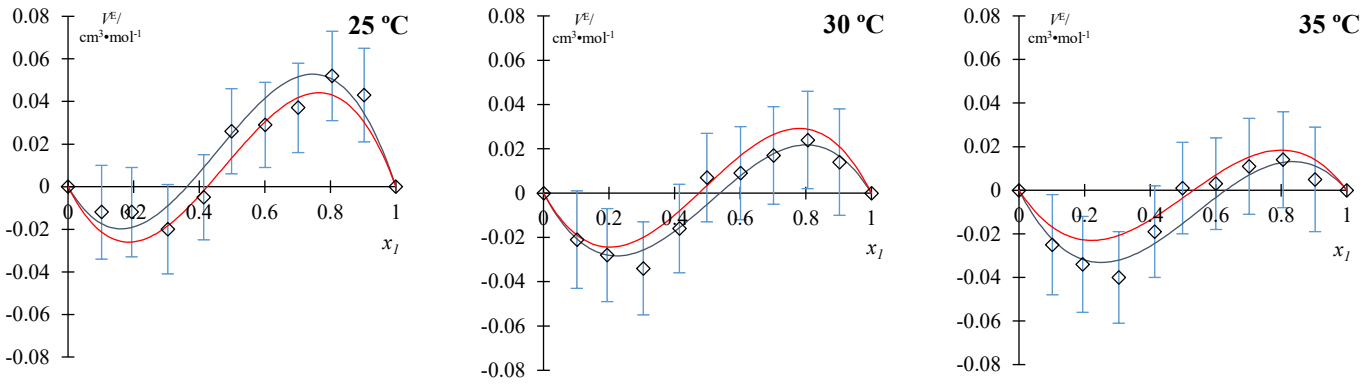

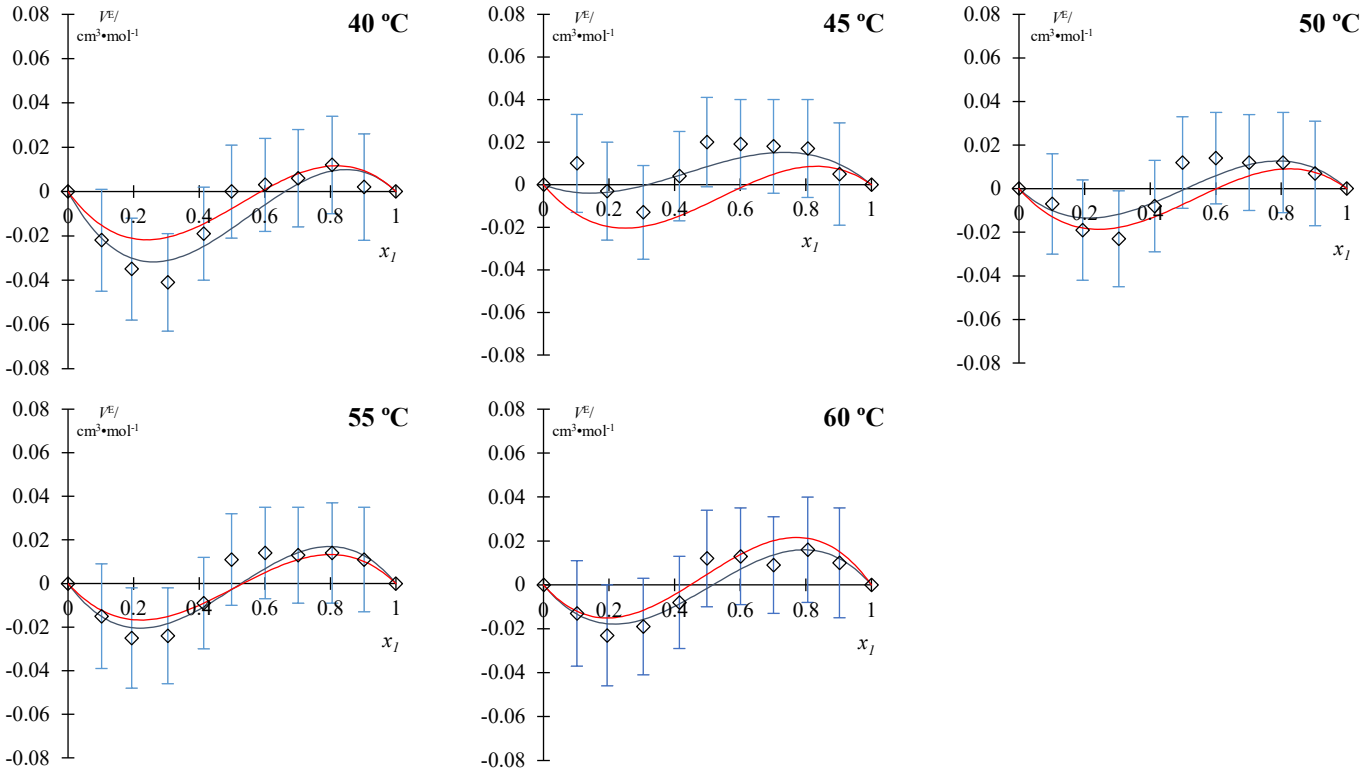

Figure 17. Dependences of the excess molar volume V^E versus concentration x_i in the trans-perfluorodecalin (1)–cis-perfluorodecalin (2) system at temperature T. Points: experimental data according to Table 25; lines: calculated data according to the Redlich-Kister equation; red: Equation (9a)—Table 28; blue: Equation (10a,b)—Table 31.

3.7.3. Ternary System

The dependence of the density ρ on BCH–trans-PFD–cis-PFD system composition at different temperatures is presented in Table 32. The liquid molar volume, V_M, of the BCH–trans-PFD–cis-PFD system was calculated according to Equation (7) and is presented in Table 33. Excess molar volume V^E of the BCH–trans-PFD–cis-PFD system was calculated according to t Equation (8) and is presented in Table 34 and Figure 18. The V_M and V^E data (Tables 33 and 34) provides the maximum standard uncertainties, u, of the values; standard uncertainties, u, for each experimental point are given in Appendix A (Tables A10 and A11, respectively).

Table 32. Dependences of density ρ on perfluoro(butylcyclohexane) (1)–trans-perfluorodecalin (2)–cis-perfluorodecalin (3) system composition x_i at temperature T and pressure P = 99.1 kPa [a].

x_1	x_2	x_3	T/°C							
			25	30	35	40	45	50	55	60
			ρ/g·cm^{-3}							
0.57402	0.21988	0.20610	1.89013	1.87891	1.86761	1.85623	1.84481	1.83331	1.82175	1.81008
0.17479	0.19519	0.63002	1.92382	1.91265	1.90139	1.89007	1.87867	1.86720	1.85569	1.84408
0.17937	0.63244	0.18819	1.91397	1.90288	1.89168	1.88044	1.86911	1.85769	1.84621	1.83466
0.18870	0.39863	0.41267	1.91787	1.90673	1.89552	1.88424	1.87287	1.86144	1.84997	1.83842
0.36974	0.40875	0.22151	1.90212	1.89101	1.87981	1.86853	1.85715	1.84571	1.83419	1.82261
0.37885	0.22255	0.39860	1.90497	1.89385	1.88261	1.87129	1.85991	1.84846	1.83691	1.82532

[a] Standard uncertainties u: $u(T)$ = 0.05 °C; $u(x_i)$ = 0.00005; $u(\rho)$ = 0.0001 g·cm^{-3}; $u(P)$ = 0.3 kPa.

Table 33. Dependences of the liquid molar volume V_M on perfluoro(butylcyclohexane) (1)–trans-perfluorodecalin (2)–cis-perfluorodecalin (3) system composition x_i at temperature T [a].

			T/°C							
x_1	x_2	x_3	25	30	35	40	45	50	55	60
			V_M/cm^{-3}·mol^{-1}							
0.57402	0.21988	0.20610	256.007	257.536	259.094	260.683	262.296	263.942	265.617	267.329
0.17479	0.19519	0.63002	243.640	245.063	246.515	247.991	249.496	251.028	252.585	254.176
0.17937	0.63244	0.18819	244.988	246.416	247.875	249.356	250.868	252.410	253.979	255.578
0.18870	0.39863	0.41267	244.669	246.099	247.554	249.036	250.548	252.087	253.650	255.243
0.36974	0.40875	0.22151	250.314	251.784	253.284	254.813	256.375	257.964	259.584	261.233
0.37885	0.22255	0.39860	250.121	251.589	253.091	254.622	256.180	257.767	259.388	261.035

[a] Standard uncertainties u: $u(T)$ = 0.05 °C; $u(x_i)$ = 0.00005; $u(V_M)$ = 0.024 cm^{-3}·mol^{-1}.

Table 34. Dependences of the excess molar volume V^E on perfluoro(butylcyclohexane) (1)–trans-perfluorodecalin (2)–cis-perfluorodecalin (3) system composition x_i at temperature T [a].

			T/°C							
x_1	x_2	x_3	25	30	35	40	45	50	55	60
			V^E/cm^{-3}·mol^{-1}							
0.57402	0.21988	0.20610	0.386	0.375	0.364	0.358	0.353	0.334	0.326	0.313
0.17479	0.19519	0.63002	0.308	0.291	0.279	0.269	0.285	0.263	0.250	0.243
0.17937	0.63244	0.18819	0.289	0.262	0.248	0.236	0.234	0.223	0.217	0.209
0.18870	0.39863	0.41267	0.344	0.324	0.308	0.297	0.305	0.287	0.275	0.262
0.36974	0.40875	0.22151	0.417	0.392	0.373	0.360	0.359	0.341	0.334	0.320
0.37885	0.22255	0.39860	0.466	0.443	0.427	0.416	0.418	0.394	0.388	0.372

[a] Standard uncertainties u: $u(T)$ = 0.05 °C; $u(x_i)$ = 0.00005; $u(V^E)$ = 0.189 cm^{-3}·mol^{-1}.

The excess molar volume data (Table 34) of the BCH–trans-PFD–cis-PFD system were correlated with the Kohler [140,141] Equation (11); the data calculated by Equation (11) for the BCH–trans-PFD–cis-PFD system are presented in Table 35. The standard deviation σ (Equation (9b)) between experimental (Table 34) and calculated by Equation (11) (Table 35) data for each temperature are given in Appendix A (Table A12).

$$V^E = \sum_{i \neq j; i,j=1}^{i,j} \left(x_i + x_j\right)^2 V_{ij}^E \quad (11)$$

where $V_{ij}^E = x_i' x_j' \sum_{l=0}^{l} a_l \left(x_i' - x_j'\right)^l$ indicates that the excess molar volume of the pseudo-binary system with composition $x_i' = x_i/\left(x_i + x_j\right)$ and $x_j' = x_j/\left(x_i + x_j\right)$; $a_l = \sum_{j=0}^{j} b_j T^j$ indicates that the temperature depended Redlich-Kister parameters; x_i represents the composition of the ternary system; b_j is calculated from binary system data parameters (listed in Tables 29–31); T represents the temperature, °C.

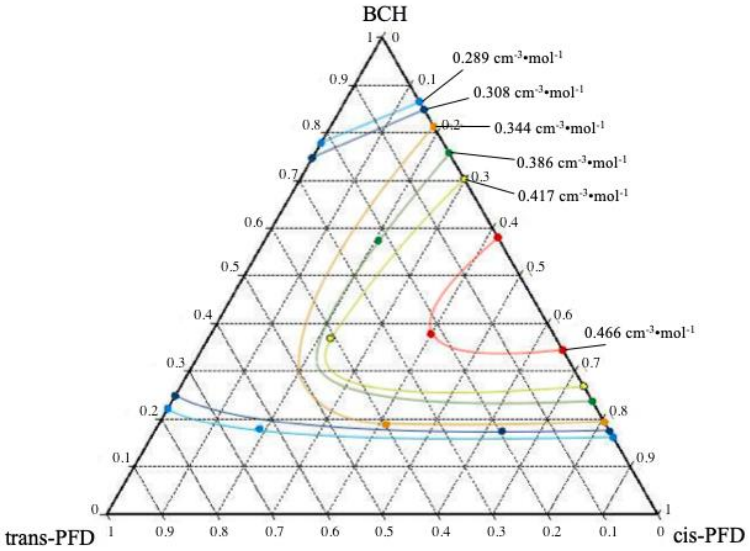

Figure 18. Dependence of the isoline of excess molar volume V^E on perfluoro(butylcyclohexane) (BCH)–trans-perfluorodecalin (trans-PFD)–cis-perfluorodecalin (cis-PFD) system composition at 25 °C according to the Tables 26–28 and 34 data.

Table 35. Calculated by Kohler Equation (11) the excess molar volume V^E_{calc} data for the perfluoro(butylcyclohexane) (1)–trans-perfluorodecalin (2)–cis-perfluorodecalin (3) system at temperature T and composition x.[a]

			T/°C							
x_1	x_2	x_3	25	30	35	40	45	50	55	60
			V^E_{calc}/cm⁻³·mol⁻¹							
0.57402	0.21988	0.20610	0.452	0.437	0.425	0.415	0.409	0.405	0.403	0.405
0.17479	0.19519	0.63002	0.270	0.260	0.251	0.245	0.241	0.238	0.238	0.239
0.17937	0.63244	0.18819	0.283	0.257	0.235	0.219	0.208	0.201	0.199	0.203
0.18870	0.39863	0.41267	0.288	0.270	0.255	0.243	0.235	0.231	0.229	0.231
0.36974	0.40875	0.22151	0.377	0.358	0.341	0.328	0.318	0.311	0.308	0.307
0.37885	0.22255	0.39860	0.414	0.399	0.386	0.375	0.366	0.360	0.355	0.352

[a] $\sigma(V^E)$ = 0.049 cm³·mol⁻¹.

4. Discussion

4.1. Spectrum Data

To verify the structures and molecular weights of the studied components, GC-MS and NMR data were obtained.

Based on the analysis of the trans-PFD and cis-PFD gas chromatography–mass spectrometry data (Figure 2), it follows that both samples weighed 462 g·mol⁻¹ and the fragmentation patterns included standard fragmentation (93—[C_3F_3], 131—[C_3F_5], 443—[$C_{10}F_{17}$] and 462—$C_{10}F_{18}$ for example), although the intensity of the patterns differed slightly from those in the literature [142]. The ^{19}F NMR spectra of the trans-PFD and cis-PFD (Figure 3b) corresponded to that reported previously [63]. Despite the fact that the ^{19}F spectrum of the cis-PFD was more complex than that for trans-PFD (Figure 3b), their ^{13}C spectra were similar (Figure 3a). The fingerprint region of trans-PFD and cis-PFD FTIR spectra are presented in Figure 4. The FTIR spectra were relatively similar if the wave numbers were overlooked (Figure 4c). The characteristic peaks of trans-PFD and cis-PFD (Figure 4) corresponded to those in the literature [115]. Meanwhile, the relative intensity of the characteristic trans-PFD and cis-PFD peaks near 1250 cm⁻¹ did not agree with those reported by Bris et al. [115]. However, a more detailed analysis of gas chromatography–mass spectrometry data (Figure 2) via NMR (Figure 3) and FTIR (Figure 4) was not

provided as their interpretation is difficult and is a separate scientific task. As the data seem to be useful, the «.mzxml», «.dx» and «.ispd» original files are provided.

4.2. Differential Scanning Calorimetry Data

Based on the analysis of the DSC data (Figure 5 and Table 2), in the case of the cis-PFD at cooling and heating, a considerable difference was observed between onset points of crystallization and melting (T_c = −17.20 °C and T_m = −6.99 °C); moreover, the crystallization average point was outside the onset and endset of the heat effect ($T_c^{endset} < T_c^{onset} < T_c^{average}$). The same situation occurred in the case of trans-PFD (T_c = 3.48 °C and T_m = 21.22 °C; $T_c^{endset} < T_c^{onset} < T_c^{average}$). The observed difference may be caused by low thermal conductivity, difficulties forming a solid phase nucleus (crystallization centers), and the resulting supercooling. However, the obtained experimental data on solid–liquid phase transition ($T_m^{cis-PFD}$ = −6.99 °C and $T_m^{trans-PFD}$ = 21.22 °C) and its heat effect ($\Delta H_m^{cis-PFD}$ = 21.35 J·g^{-1} and $\Delta H_m^{trans-PFD}$ = 38.41 J·g^{-1}) agree with that presented in the literature [143] ($T_m^{cis-PFD}$ = −6.55 °C and $T_m^{trans-PFD}$ = 21.46 °C; $\Delta H_m^{cis-PFD}$ = 22.30 J·g^{-1} and $\Delta H_m^{trans-PFD}$ = 38.87 J·g^{-1}). The melting temperature data were also presented by Smith [123] ($T_m^{cis-PFD}$ = −7.0 °C and $T_m^{trans-PFD}$ = 17.5 °C), however, the samples exhibited low purity (cis-PFD [123] > 95% mass., trans-PFD [123] > 90% mass.).

Following cooling and heating of the samples among the crystallization and melting characteristic peaks, the DSC data showed additional heat effects:

- In the case of cis-PFD heating, two effects were absent during cooling. The first (−39.11 °C) correlates to the solid-solid phase transition (c_{II}/c_I) temperature [143] (−40.65 °C); their heat effects differed ($\Delta H_{c_{II}/c_I}^{exp}$ = 0.60 J·g^{-1} and $\Delta H_{c_{II}/c_I}^{lit}$ = 9.18 J·g^{-1}). The second belongs to the −95.69 °C to −87.60 °C temperature range and is not found in the literature; it likely corresponds to the glass transition effect. The conclusion agrees with the T_g/T_m = 2/3 empirical rule [144], where the temperature is in Kelvin scale.
- In the case of trans-PFD cooling, there is a relaxation effect at −0.90 °C subsequent to the crystallization caused by supercooling. In the case of trans-PFD heating, there is a heat effect in the temperature range from −96.57 °C to −85.87 °C, which is absent during cooling. This likely corresponds to the glass transition effect that agrees with the two-thirds empirical rule [144].

4.3. Viscosity

The data obtained in the present work for trans-PFD and cis-PFD are equivalent to those previously reported for BCH and MBCN [130]. The compounds showed Newtonian behavior (Figure 6), with «zero» shear viscosity values of $\eta_{trans-PFD}^{25\,^{\circ}C}$ = 49.4 × 10^{-4} Pa·s and $\eta_{cis-PFD}^{25\,^{\circ}C}$ = 69.4 × 10^{-4} Pa·s (Table 3). As the temperature increased, the $\eta_{trans-PFD}^{T}$ and $\eta_{cis-PFD}^{T}$ values decreased (Figure 7a). The $\eta = f\left(\frac{1}{T}\right)$ function was linear (Figure 7b). The $\eta_{trans-PFD}^{T}$ and $\eta_{cis-PFD}^{T}$ data correlated with the Arrhenius Equation (1). The coefficients of the Arrhenius equation are listed in Table 4.

In the case of trans-PFD, crystallization at 9.3 °C was detected during the continuous temperature scanning mode (Figure 8). The rotational rheometry data disagreed with the DSC data (Table 2) as the experiment was carried out under constant shear conditions. At the process's initial stage, the solid phase nucleus (crystallization centers) was destroyed. As a result, the crystallization was detected at lower temperatures.

The dependences of viscosity on the shear rate at 25 °C and temperature of the MBCN, BCH, trans-PFD, and cis-PFD are shown in Figure 9. In the investigated shear rate and temperature ranges, the viscosity order of the components was as follows: $\eta_{cis-PFD} > \eta_{trans-PFD} > \eta_{MBCN} > \eta_{BCH}$.

Deepika [101] provided data on the dependence of the dynamic viscosity at different temperatures ($\eta_{PFD}^{25\,^{\circ}C}$ = 56.47 Pa·s × 10^{-4}, for example) and apparent activation energy (E_a^{PFD} = 19,920 J·mol^{-1}) for the viscous flow of the «pure perfluorodecalin» isomeric

composition of which is not given; the data are within the range of values determined in the present work for trans-PFD ($\eta^{25\,^{\circ}C}_{trans-\,PFD} = 49.4$ Pa·s × 10^{-4}, $E_a^{trans-PFD}$ = 17,944.3 J·mol^{-1}) and cis-PFD ($\eta^{25\,^{\circ}C}_{cis-\,PFD} = 69.3$ Pa·s × 10^{-4}, $E_a^{cis-PFD}$ = 24,036.6 J·mol^{-1}) (Tables 3 and 4).

Haszeldine [104] also provides data on PFD viscosity in the 25 to 80 °C range, however, the isomeric composition is not given; the data are similar to the experimental values obtained in the present work for trans-PFD (Table 3): $\Delta\eta^{25\,^{\circ}C}_{trans-\,PFD} = 49.4^{exp} - 51.4^{lit} = -2.0$ Pa·s × 10^{-4}; $\Delta\eta^{35\,^{\circ}C}_{trans-\,PFD} = 38.2^{exp} - 37.6^{lit} = 0.6$ Pa·s × 10^{-4}; $\Delta\eta^{45\,^{\circ}C}_{trans-\,PFD} = 31.2^{exp} - 28.6^{lit} = 2.2$ Pa·s × 10^{-4}. A similar situation was observed when comparing the data from Freire [103] with those in Table 3.

4.4. Saturated Vapor Pressure

The obtained dependences of the saturated vapor pressure for trans-PFD (Table 5) and cis-PFD (Table 6) on temperature showed that T_b difference remained relatively intact ΔT_b^P = [0.3; 1.4] °C; the Antoine Equation (2) and regressed parameters (Table 7) provide a proper correlation of the experimental data (Figure 10a,b). Considering the experimental uncertainty, the measured values for the dependence of saturated vapor pressure on temperature for trans-PFD (Table 5) and cis-PFD (Table 6) were generally in agreement with the literature data [90,123,136,145]. However, there were some inconsistencies for the boiling point row of the components under study: $\left(T_b^{trans-PFD} < T_b^{cis-PFD} < T_b^{BCH}\right)$ [123,136,145] and $\left(T_b^{trans-PFD} < T_b^{BCH} < T_b^{cis-PFD}\right)^{exp}$. Note that in Dias [90] a mixture of trans-PFD and cis-PFD in an unknown ratio was used; in Smith [123] the purity of the investigated samples was relatively low (cis-PFD > 95% mass., trans-PFD > 90% mass.), and in the Gervits [136] and Varushchenko [145] the purity was unspecified.

From Figure 10c, it follows that the $P = f(T)$ dependence of the MBCN significantly differed from other components, and trans-PFD, cis-PFD, and BCH are close-boiling substances. The question of the presence of Bancroft's point for trans-PFD, cis-PFD, and BCH remains unclear, as the temperature uncertainty was within the range of measurable differences. In the case of Bancroft's point being present, the system is characterized by an azeotrope under certain conditions. Moreover, the Bancroft point is a condition for the transition boundary tangential azeotropy to internal tangential azeotropy (and inverse) in the case of binary biazeotropic systems [146].

Since MBCN is a mixture of diastereomers, the ratio changes of which may lead to changes in the properties of the sample, MBCN was removed from further consideration.

4.5. Refractive Index

The dependences of the trans-PFD (Table 8) and cis-PFD (Table 9) refractive index were linear and inversely proportional to temperature (Figure 11). Both were described by Equation (3), and the coefficients are presented in Table 10. In the case of trans-PFD, the dependence of the refractive index was obtained for the 25 to 60 °C range as it is limited by the melting point value. Data on the refractive index value for PFD without specifying the isomeric composition were also presented by Haszeldine [104]. Compared with data reported by Smith [123] (trans-PFD $\Delta n_D^{18\,^{\circ}C} = 1.3145^{exp}_{eq.3} - 1.3148^{lit} = -0.0003$ and cis-PFD $\Delta n_D^{18\,^{\circ}C} = 1.3180^{exp}_{Table\ 9} - 1.3179^{lit} = 0.0001$), the values were relatively similar; however, the purity of the investigated samples was relatively low (cis-PFD [123] > 95% mass., trans-PFD [123] > 90% mass.).

The differences in the refractive index of the trans-PFD–cis-PFD, BCH–trans-PFD, and BCH–cis-PFD systems were sufficient to construct calibration curves to determine the composition of the systems on refractive index (Table 11). The dependences of the refractive index on the system's composition (Equation (4)) were composed from the data shown in Figure 12. The coefficients of Equation (4) are listed in Table 12. The acceptable standard uncertainties were: $u\left(x_i^{n_D}\right) = 0.027$ mole fraction at 25 °C for the trans-PFD–cis-PFD system; $u\left(x_i^{n_D}\right) = 0.0063$ mole fraction at 15 °C for the BCH–trans-PFD system;

$u(x_i^{n_D}) = 0.0045$-mole fraction at 15 °C for the BCH–cis-PFD system. For the BCH–trans-PFD–cis-PFD three-component system, the dependences of the refractive index on composition and temperature were obtained (Table 13), and the behavior of the refractive index isolines at T = 15 °C were plotted (Figure 13). In the range of investigating concentration, the dependencies had a linear behavior.

4.6. Density and Liquid Molar Volume

The dependencies of the trans-PFD (Table 14) and cis-PFD (Table 15) density and liquid molar volume were linear and inversely/directly proportional to the temperature, respectively (Figure 14). Both were described by Equations (5) and (6); the equation coefficients are presented in Table 16. In the case of trans-PFD, the dependences of the density and liquid molar volume were obtained for the 25 to 60 °C range as it is limited by the melting point value. Following the example of the viscosity data, comparing the results of the present work with those reported in the literature [90,101,102,104] is difficult due to the absence of the PFD isomeric composition. If the data is compared with that of Varushchenko [145] (trans-PFD $\Delta\rho^{25\,^{\circ}C} = 1.92344^{exp}_{Table\ 14} - 1.9241^{lit} = -0.00066$ g·cm^{-3} and cis-PFD $\Delta\rho^{25\,^{\circ}C} = 1.94613^{exp}_{Table\ 15} - 1.9414^{lit} = 0.00473$ g·cm^{-3}), the values differ in the third digit, but the purity of the investigated samples was unspecified [145].

The dependencies of the density value of the BCH–cis-PFD (Table 17), BCH–trans-PFD (Table 18), and trans-PFD–cis-PFD (Table 19) system's composition were used to calculate the liquid molar volume (Tables 20–22, respectively) and excess molar volume (Tables 23–25, respectively). To create a mathematical model of the excess molar volume versus composition at different temperatures the data were correlated with Equation (9a) equation system (10). The number of parameters in Equation (9a) was sufficient to ensure that the $\sigma(V^E)$ changed negligently with further increases in the value of i; for the BCH–cis-PFD system, i = 3 (Table 26); for the BCH–trans-PFD system, i = 4 (Table 27); for the trans-PFD–cis-PFD system, i = 1 (Table 28). The temperature parameters of the Redlich-Kister equation according to the Equation (10) system are presented in: Table 29 for the BCH–cis-PFD system, Table 30 for the BCH–trans-PFD system, and Table 31 for the trans-PFD–cis-PFD system. By analogy with Equation (9a), the number of parameters for Equation (10) was sufficient so that the $\sigma(V^E)$ changed negligently with further increases in the i and j values. For the BCH–cis-PFD and BCH–trans-PFD systems, the comparison of experimental (Tables 23 and 24) and calculated by Equation (9a) (Tables 26 and 27) and Equation (10) (Tables 29 and 30) values showed that both models had negligible mutual deviation and described the data within the experimental uncertainty (Figures 15 and 16). The values of excess molar volume in the trans-PFD–cis-PFD system were an order of magnitude lower than in the other two systems under consideration. In the case of the trans-PFD–cis-PFD system, the measured values of the excess molar volume were within the experimental uncertainty (Table 25); both models (Equation (9a) Table 28, Equation (10) Table 31) had mutual deviation but described the data within the experimental uncertainty (Figure 17). Thus, all the correlations could be considered satisfactory.

The dependency of the density value on the BCH–trans-PFD–cis-PFD (Table 32) system's composition was used to calculate the liquid molar volume (Table 33) and excess molar volume (Table 34). The excess molar volume data were correlated with Equation (11) using the temperature-dependent parameters (Tables 29–31). The data calculated by the Kohler Equation (11) on the excess molar volume for the BCH–trans-PFD–cis-PFD system are listed in Table 35. From the comparison of Tables 34 and 35 data, it can be concluded that the model describes the experimental data within the experimental standard uncertainty. The curves of the isolines of the excess molar volume in the BCH–trans-PFD–cis-PFD system are shown in Figure 18. The highest values of excess molar volume corresponded to the composition of the BCH–cis-PFD close to the equimolar.

5. Conclusions

The obtained experimental data partially supplement and, in many aspects, extend the information presented in the literature. First, the new experimental data provide are background information and a starting point for further research. For example, the obtained data are necessary for engineering calculations of individual apparatuses (calculation of mass transfer coefficients, hydrodynamic properties, heat exchange devices, Rayleigh, Prandtl, Nusselt, and Reynolds numbers) and the process in general (engineering analysis or mathematical modeling with modern software complexes, such as Aspen Plus and others). In addition, these data may interest researchers of both allied and very distant field sciences.

Supplementary Materials: The following supporting information can be downloaded at: https://www.mdpi.com/article/10.3390/pr11113208/s1, ^{19}F NMR, FTIR and GC-MS original files for cis-perfluorodecalin and trans-perfluorodecalin.

Author Contributions: Conceptualization, E.V.L. and A.V.P.; methodology, E.V.L. and A.V.P.; validation, E.V.L. and A.V.P.; formal analysis, E.V.L. and A.V.P.; investigation, E.V.L., A.V.P. and A.V.K.; writing—original draft preparation, A.V.P.; writing—review and editing, E.V.L., A.V.P., N.N.K., Y.A.Z. and A.A.V.; visualization, A.V.P.; supervision, A.V.P., E.V.L. and A.A.V.; project administration, A.V.P., E.V.L. and N.N.K.; funding acquisition, A.A.V., N.N.K. and Y.A.Z. All authors have read and agreed to the published version of the manuscript.

Funding: This study was financially supported by the Russian Science Foundation, project no. 22-29-00791, https://rscf.ru/en/project/22-29-00791/ (access date 9 November 2023).

Data Availability Statement: Data is contained within the article or Supplementary Materials.

Acknowledgments: NMR and chromatography–mass spectrometry data were obtained using the equipment of the JRC PMR IGIC RAS.

Conflicts of Interest: The authors declare no competing financial interests.

Nomenclature

Reductions	
BCH	perfluoro(butylcyclohexane)
DSC	differential scanning calorimetry
FTIR	Fourier transform infrared spectrum
GC	gas chromatography
MBCN	perfluoro(7-methylbicyclo[4.3.0]nonane)
NMR	nuclear magnetic resonance
PFD	perfluorodecalin
Symbols	
$A_i^{n_D}$, $B_i^{n_D}$	coefficients of Equation (3)
A_i^P, B_i^P, C_i^P	coefficients of Antoine equation
A_i^ρ, B_i^ρ	coefficients of Equation (6)
$a_0^{n_D}$, $a_1^{n_D}$, $a_2^{n_D}$	coefficients of Equation (4).
a_i	Redlich-Kister parameters
b_j	parameters of the Equation (10b)
ΔC_p	heat capacity change, J·g^{-1}·K^{-1}
d	number of compositions studied
E_a	apparent activation energy for the viscous flow, J·mol^{-1}
f	function
H	enthalpy, J·g^{-1}
M	molecular weight, g·mole^{-1}
m	sample weight, g
ñ	number of terms used in the regression
n_D	refractive index
P	pressure, kPa
R = 8.314	molar gas constant, J·K^{-1}·mol^{-1}

T	temperature, °C or K
u	standard uncertainty
u_r	relative uncertainty
V_M	liquid molar volume, $cm^3 \cdot mol^{-1}$
V^E	excess molar volume, $cm^3 \cdot mol^{-1}$
x_i	phase composition, mole fraction
Greek letters	
$\dot{\gamma}$	shear rate, s^{-1}
Δ	changes
$\sum$	sum
η	shear viscosity, Pa·s
η_0	constant parameter of Equation (1), Pa·s
ρ	density, $g \cdot cm^{-3}$
σ	standard deviations
Subscripts	
b	boiling point
c	crystallization
D	distillate
exp	experimental
calc	calculated
g	glass transition
i, j	components
lit	literature
max	maximum
min	minimum
m	melting
W	bottom

Appendix A

Table A1. Dependences of the standard deviation values of liquid molar volume $u(V_M)$ on perfluoro(butylcyclohexane) (1)–cis-perfluorodecalin (2) system composition x_i at temperature T.

x_1	T/°C									
	15	**20**	**25**	**30**	**35**	**40**	**45**	**50**	**55**	**60**
	$u(V_M)/cm^{-3} \cdot mol^{-1}$									
0	0.012	0.012	0.012	0.012	0.012	0.013	0.013	0.013	0.013	0.013
0.10343	0.021	0.021	0.022	0.022	0.022	0.022	0.022	0.022	0.023	0.023
0.17164	0.014	0.014	0.014	0.015	0.015	0.015	0.015	0.015	0.015	0.016
0.28538	0.022	0.022	0.022	0.022	0.022	0.022	0.023	0.023	0.023	0.023
0.31744	0.016	0.017	0.017	0.017	0.017	0.017	0.017	0.018	0.018	0.018
0.35826	0.019	0.019	0.019	0.019	0.020	0.020	0.020	0.020	0.020	0.021
0.37933	0.019	0.019	0.019	0.020	0.020	0.020	0.020	0.020	0.020	0.021
0.39919	0.019	0.019	0.019	0.020	0.020	0.020	0.020	0.020	0.020	0.021
0.44022	0.019	0.019	0.019	0.020	0.020	0.020	0.020	0.020	0.021	0.021
0.50224	0.019	0.019	0.020	0.020	0.020	0.020	0.020	0.020	0.021	0.021
0.60547	0.019	0.020	0.020	0.020	0.020	0.020	0.020	0.021	0.021	0.021
0.69350	0.022	0.023	0.023	0.023	0.023	0.023	0.023	0.024	0.024	0.024
0.80202	0.023	0.023	0.023	0.023	0.023	0.023	0.024	0.024	0.024	0.024
0.88860	0.023	0.023	0.023	0.023	0.023	0.024	0.024	0.024	0.024	0.025
1	0.014	0.014	0.014	0.015	0.015	0.015	0.015	0.015	0.015	0.016

Table A2. Dependences of the standard deviation values of liquid molar volume $u(V_M)$ on perfluoro(butylcyclohexane) (1)–trans-perfluorodecalin (2) system composition x_i at temperature T.

x_1	T/°C							
	25	**30**	**35**	**40**	**45**	**50**	**55**	**60**
	$u(V_M)$/cm^{-3}·mol^{-1}							
0	0.012	0.013	0.013	0.013	0.013	0.013	0.013	0.014
0.10688	0.017	0.017	0.017	0.017	0.017	0.017	0.018	0.018
0.19419	0.017	0.017	0.017	0.017	0.017	0.018	0.018	0.018
0.29614	0.019	0.020	0.020	0.020	0.020	0.020	0.020	0.021
0.40516	0.020	0.020	0.020	0.020	0.020	0.020	0.021	0.021
0.49698	0.020	0.020	0.020	0.020	0.020	0.021	0.021	0.021
0.59993	0.020	0.020	0.020	0.020	0.021	0.021	0.021	0.021
0.69763	0.023	0.023	0.023	0.023	0.024	0.024	0.024	0.024
0.80471	0.023	0.023	0.023	0.024	0.024	0.024	0.024	0.024
0.89712	0.026	0.026	0.026	0.027	0.027	0.027	0.027	0.028
1	0.014	0.015	0.015	0.015	0.015	0.015	0.015	0.016

Table A3. Dependences of the standard deviation values of liquid molar volume $u(V_M)$ on trans-perfluorodecalin (1)–cis-perfluorodecalin (2) system composition x_i at temperature T.

x_1	T/°C							
	25	**30**	**35**	**40**	**45**	**50**	**55**	**60**
	$u(V_M)$/cm^{-3}·mol^{-1}							
0	0.012	0.012	0.012	0.013	0.013	0.013	0.013	0.013
0.10198	0.012	0.012	0.013	0.013	0.013	0.013	0.013	0.013
0.19411	0.012	0.012	0.013	0.013	0.013	0.013	0.013	0.013
0.30439	0.012	0.012	0.013	0.013	0.013	0.013	0.013	0.013
0.41417	0.012	0.012	0.013	0.013	0.013	0.013	0.013	0.013
0.49848	0.012	0.012	0.013	0.013	0.013	0.013	0.013	0.013
0.60085	0.012	0.013	0.013	0.013	0.013	0.013	0.013	0.013
0.70172	0.012	0.013	0.013	0.013	0.013	0.013	0.013	0.013
0.80539	0.012	0.013	0.013	0.013	0.013	0.013	0.013	0.014
0.90273	0.012	0.013	0.013	0.013	0.013	0.013	0.013	0.014
1	0.012	0.013	0.013	0.013	0.013	0.013	0.013	0.014

Table A4. Dependences of the standard deviation values of excess molar volume $u(V^E)$ on perfluoro(butylcyclohexane) (1)–cis-perfluorodecalin (2) system composition x_i at temperature T.

x_1	T/°C									
	15	**20**	**25**	**30**	**35**	**40**	**45**	**50**	**55**	**60**
	$u(V^E)$/cm^{-3}·mol^{-1}									
0.10343	0.030	0.030	0.030	0.031	0.031	0.031	0.031	0.031	0.032	0.032
0.17164	0.019	0.019	0.019	0.020	0.020	0.020	0.020	0.020	0.020	0.021
0.28538	0.030	0.030	0.030	0.030	0.030	0.030	0.031	0.031	0.031	0.031
0.31744	0.021	0.022	0.022	0.022	0.022	0.022	0.023	0.023	0.024	0.024
0.35826	0.025	0.025	0.026	0.026	0.026	0.027	0.027	0.027	0.027	0.028
0.37933	0.025	0.025	0.026	0.026	0.026	0.027	0.027	0.027	0.027	0.028
0.39919	0.025	0.025	0.026	0.026	0.026	0.027	0.027	0.027	0.027	0.028
0.44022	0.025	0.025	0.026	0.026	0.026	0.027	0.027	0.027	0.028	0.028
0.50224	0.025	0.026	0.026	0.026	0.027	0.027	0.027	0.027	0.028	0.028
0.60547	0.026	0.026	0.027	0.027	0.027	0.027	0.027	0.028	0.028	0.028
0.69350	0.030	0.031	0.031	0.031	0.031	0.031	0.031	0.032	0.032	0.033
0.80202	0.031	0.031	0.031	0.032	0.032	0.032	0.033	0.033	0.033	0.033
0.88860	0.032	0.032	0.032	0.032	0.032	0.033	0.033	0.033	0.033	0.034

Table A5. Dependences of the standard deviation values of excess molar volume $u(V^E)$ on perfluoro(butylcyclohexane) (1)–trans-perfluorodecalin (2) system composition x_i at temperature T.

x_1	T/°C							
	25	30	35	40	45	50	55	60
	$u(V^E)$/cm^{-3}·mol^{-1}							
0.10688	0.023	0.023	0.023	0.023	0.024	0.024	0.024	0.024
0.19419	0.022	0.023	0.023	0.023	0.023	0.024	0.024	0.024
0.29614	0.026	0.026	0.026	0.027	0.027	0.027	0.027	0.028
0.40516	0.026	0.026	0.026	0.027	0.027	0.027	0.027	0.028
0.49698	0.026	0.026	0.027	0.027	0.027	0.027	0.028	0.028
0.59993	0.026	0.027	0.027	0.027	0.027	0.028	0.028	0.028
0.69763	0.031	0.031	0.031	0.032	0.032	0.032	0.033	0.033
0.80471	0.031	0.032	0.032	0.032	0.033	0.033	0.033	0.033
0.89712	0.036	0.037	0.037	0.037	0.037	0.038	0.038	0.038

Table A6. Dependences of the standard deviation values of excess molar volume $u(V^E)$ on trans-perfluorodecalin (1)–cis-perfluorodecalin (2) system composition x_i at temperature T.

x_1	T/°C							
	25	30	35	40	45	50	55	60
	$u(V^E)$/cm^{-3}·mol^{-1}							
0.10198	0.022	0.022	0.023	0.023	0.023	0.023	0.024	0.024
0.19411	0.021	0.021	0.022	0.023	0.023	0.023	0.023	0.023
0.30439	0.021	0.021	0.021	0.022	0.022	0.022	0.022	0.022
0.41417	0.020	0.020	0.021	0.021	0.021	0.021	0.021	0.021
0.49848	0.020	0.020	0.021	0.021	0.021	0.021	0.021	0.022
0.60085	0.020	0.021	0.021	0.021	0.021	0.021	0.021	0.022
0.70172	0.021	0.022	0.022	0.022	0.022	0.022	0.022	0.022
0.80539	0.021	0.022	0.022	0.022	0.023	0.023	0.023	0.024
0.90273	0.022	0.024	0.024	0.024	0.024	0.024	0.024	0.025

Table A7. Standard deviations σ (Equation (9b)) between experimental (Table 23) and calculated by Equation (10) (Table 29) data for the perfluoro(butylcyclohexane) (1)–trans-perfluorodecalin (2) system.

T/°C	$\sigma(V^E)$/cm^{-3}·mol^{-1}
15	0.023
20	0.020
25	0.020
30	0.019
35	0.019
40	0.018
45	0.018
50	0.021
55	0.019
60	0.020

Table A8. Standard deviations σ (Equation (9b)) between experimental (Table 24) and calculated by Equation (10) (Table 30) data for the perfluoro(butylcyclohexane) (1)–cis-perfluorodecalin (2) system.

T/°C	$\sigma(V^E)$/cm^{-3}·mol^{-1}
25	0.019
30	0.015
35	0.013
40	0.012
45	0.012
50	0.013
55	0.013
60	0.011

Table A9. Standard deviations σ (Equation (9b)) between experimental (Table 25) and calculated by Equation (10) (Table 31) data for the trans-perfluorodecalin (1)–cis-perfluorodecalin (2) system.

T/°C	$\sigma(V^E)$/cm^{-3}·mol^{-1}
25	0.010
30	0.009
35	0.010
40	0.011
45	0.020
50	0.010
55	0.008
60	0.007

Table A10. Dependences of the standard deviation values of liquid molar volume $u(V_M)$ on perfluoro(butylcyclohexane) (1)–trans-perfluorodecalin (2)–cis-perfluorodecalin (3) system composition x_i at temperature T.

			T/°C							
x_1	x_2	x_3	25	30	35	40	45	50	55	60
			$u(V_M)$/cm^{-3}·mol^{-1}							
0.57402	0.21988	0.20610	0.022	0.022	0.023	0.023	0.023	0.023	0.023	0.024
0.17479	0.19519	0.63002	0.021	0.021	0.022	0.022	0.022	0.022	0.022	0.023
0.17937	0.63244	0.18819	0.021	0.021	0.021	0.022	0.022	0.022	0.022	0.022
0.18870	0.39863	0.41267	0.020	0.020	0.020	0.020	0.021	0.021	0.021	0.021
0.36974	0.40875	0.22151	0.020	0.021	0.021	0.021	0.021	0.021	0.022	0.022
0.37885	0.22255	0.39860	0.020	0.020	0.021	0.021	0.021	0.021	0.021	0.022

Table A11. Dependences of the standard deviation values of excess molar volume $u(V^E)$ on perfluoro(butylcyclohexane) (1)–trans-perfluorodecalin (2)–cis-perfluorodecalin (3) system composition x_i at temperature T.

			T/°C							
x_1	x_2	x_3	25	30	35	40	45	50	55	60
			$u(V^E)$/cm^{-3}·mol^{-1}							
0.57402	0.21988	0.20610	0.183	0.184	0.185	0.186	0.186	0.187	0.187	0.189
0.17479	0.19519	0.63002	0.181	0.182	0.182	0.184	0.184	0.184	0.185	0.186
0.17937	0.63244	0.18819	0.179	0.181	0.181	0.182	0.182	0.183	0.183	0.185
0.18870	0.39863	0.41267	0.173	0.174	0.174	0.175	0.176	0.176	0.177	0.178
0.36974	0.40875	0.22151	0.174	0.176	0.176	0.177	0.177	0.177	0.178	0.180
0.37885	0.22255	0.39860	0.173	0.174	0.175	0.176	0.176	0.177	0.177	0.178

Table A12. Standard deviations σ (Equation (9b)) between experimental (Table 34) and calculated by Equation (11) (Table 35) data for the perfluoro(butylcyclohexane) (1)–trans-perfluorodecalin (2) system–cis-perfluorodecalin (3) system.

T/°C	$\sigma(V^E)$/cm^{-3}·mol^{-1}
25	0.047
30	0.043
35	0.041
40	0.040
45	0.050
50	0.043
55	0.041
60	0.041

References

1. Maximize Market Research PVT. LTD. *Perfluorocarbons Market—Global Industry Analysis and Forecast (2023–2029)//Report ID 60132*; Maximize Market Research PVT. LTD.: Pune, India, 2023.
2. Clark, L.C.; Wesseler, E.P.; Kaplan, S.; Emory, C.; Moore, R.; Denson, D. *Intravenous-Infusion of Cis-Trans Perfluorodecalin Emulsions in Rhesus-Monkey*; ACS Symposium Series; ACS Publications: Washington, DC, USA, 1976; pp. 135–170.
3. Chaplygina, Z.A.; Kuznetsova, I.N.; Domracheva, V.S.; Gokhman, N.S.; Maksimov, B.N.; Panshina, N.G.; Pankratova, I.G. Changes in Oxygen-Supply Levels in Rats after Exchange Blood-Transfusion with Perfluorodecalin Emulsion. *Bull. Exp. Biol. Med.* **1980**, *90*, 1513–1516. https://doi.org/10.1007/BF00834080.
4. Guaitani, A.; Villa, P.; Bartosek, I. Effect of Perfluorodecalin on the Microsomal Mono-Oxygenase System in Perfused Rat Livers. *Xenobiotica* **1983**, *13*, 39–45. https://doi.org/10.3109/00498258309052213.
5. Matvienko, V.P.; Gusenova, F.M.; Afonin, N.I.; Aprosin, N.Y.D.; Sidlyarov, D.P. Micro-Circulation Parameters in the Experimental-Therapy of Acute Hemorrhage by Infusion of the Blood Substitute, Oxygen Carrier, Based on Perfluorodecalin. *Gematol. I Transfuziol.* **1983**, *28*, 38–41.
6. Khlopushina, T.G.; Kovalev, I.E.; Lysenkova, E.M. Effect of Perfluorodecalin and Perfluorotributylamine on the Cytochrome-P-450 System of the Liver. *Biochem.-Mosc.* **1986**, *51*, 574–577.
7. Grishanova, A.Y.; Obraztsov, V.V.; Shekhtman, D.G.; Lyakhobich, V. V Phenobarbital Type of Induction of Cytochrome-P-450 of Liver-Microsomes by Perfluorodecalin. *Biochem.-Mosc.* **1987**, *52*, 981–985.
8. Chubb, C.; Draper, P. Efficacy of Perfluorodecalin as an Oxygen Carrier for Mouse and Rat Testes Perfused Invitro. *Proc. Soc. Exp. Biol. Med.* **1987**, *184*, 489–494.
9. Huang, R.; Levin, S.S.; Schleyer, H.; Cooper, D.Y.; Mukherji, B.; Sloviter, H.A. Alteration by Perfluorodecalin of Hepatic-Metabolism and Excretion of Phenobarbital. *Biochem. Pharmacol.* **1988**, *37*, 3761–3764.
10. Grishanova, A.Y.; Gutkina, N.I.; Mishin, V.M. Comparative Characterization of Isolated Forms of Cytochrome-P-450 Inducible by Phenobarbital and Perfluorodecalin. *Biochem.-Mosc.* **1988**, *53*, 312–320.
11. Putyatina, T.K.; Aprosin, Y.D.; Afonin, N.I. On the Possibility of Prolongation of the Time of Perfluorodecalin Emulsion Circulation in the Blood Bed of Rats. *Gematol. I Transfuziol.* **1988**, *33*, 25–28.
12. Mishin, V.M.; Obraztsov, V.V.; Grishanova, A.Y.; Gutkina, N.I.; Shekhtman, D.G.; Khatsenko, O.G.; Lyakhovich, V. V The Phenobarbital-Type Induction of Rat-Liver Microsomal Monooxygenases by Perfluorodecalin. *Chem. Biol. Interact.* **1989**, *72*, 143–155. https://doi.org/10.1016/0009-2797(89)90024-0.
13. Adrianov, N.V.; Archakov, A.I.; Zigler, M. Induction of Cytochrome-P-450 by Perfluorodecalin in Mouse-Liver Microsomes. *Bull. Exp. Biol. Med.* **1989**, *108*, 1098–1101. https://doi.org/10.1007/BF00840646.
14. Branca, D.; Giron, F.; Conte, L.; Vincenti, E.; Scutari, G. Energetic Behavior of Mitochondria Isolated from Rat Livers Perfused with a Perfluorodecalin + N,N-Perfluorodiethylcyclohexylamine Emulsion. *Biochem. Pharmacol.* **1989**, *38*, 3045–3048. https://doi.org/10.1016/0006-2952(89)90013-0.
15. Kovalev, I.E.; Rubtsova, E.R.; Podymova, N.G.; Filatova, I. V Immunotropic Activity of Perfluorodecalin and Perfluorotributylamine. *Khimiko-Farmatsevticheskii Zhurnal* **1989**, *23*, 135–139.
16. Luyckx, G.; Vandenbosch, A.; Ceulemans, J. A Search for Pure Compounds Suitable for Use as Matrix in Spectroscopic Studies of Radiation-Produced Radical Cations. 2. Perfluoromethylcyclohexane and Perfluorodecalin. *Spectrosc. Lett.* **1986**, *19*, 207–222. https://doi.org/10.1080/00387018608069233.
17. Watson, A.J.; Liddicoat, M.I.; Ledwell, J.R. Perfluorodecalin and Sulfur-Hexafluoride as Purposeful Marine Tracers—Some Deployment and Analysis Techniques. *Deep-Sea Res. Part A-Oceanogr. Res. Pap.* **1987**, *34*, 19–31. https://doi.org/10.1016/0198-0149(87)90118-X.
18. Popkova, N.I.; Yushchenko, A.A.; Yurkiv, V.A.; Irtuganova, O.A. Functional-Characteristics of the Antioxidative System of Mycobacteria Grown on Media Modified by Perfluorodecalin. *Bull. Exp. Biol. Med.* **1988**, *105*, 215–217. https://doi.org/10.1007/BF00835698.

19. Anthony, P.; Davey, M.R.; Power, J.B.; Washington, C.; Lowe, K.C. Synergistic Enhancement of Protoplast Growth by Oxygenated Perfluorocarbon and Pluronic F-68. *Plant Cell Rep.* **1994**, *13*, 251–255. https://doi.org/10.1007/BF00233314.
20. Laudien, J.; Groß-Heitfeld, C.; Mayer, C.; de Groot, H.; Kirsch, M.; Ferenz, K.B. Perfluorodecalin-Filled Poly(n-Butyl-Cyanoacrylate) Nanocapsules as Potential Artificial Oxygen Carriers: Preclinical Safety and Biocompatibility. *J. Nanosci. Nanotechnol.* **2015**, *15*, 5637–5648. https://doi.org/10.1166/jnn.2015.10044.
21. Wrobeln, A.; Schlüter, K.D.; Linders, J.; Zähres, M.; Mayer, C.; Kirsch, M.; Ferenz, K.B. Functionality of Albumin-Derived Perfluorocarbon-Based Artificial Oxygen Carriers in the Langendorff-Heart. *Artif. Cells Nanomed. Biotechnol.* **2017**, *45*, 723–730. https://doi.org/10.1080/21691401.2017.1284858.
22. Wrobeln, A.; Laudien, J.; Groß-Heitfeld, C.; Linders, J.; Mayer, C.; Wilde, B.; Knoll, T.; Naglav, D.; Kirsch, M.; Ferenz, K.B. Albumin-Derived Perfluorocarbon-Based Artificial Oxygen Carriers: A Physico-Chemical Characterization and First in Vivo Evaluation of Biocompatibility. *Eur. J. Pharm. Biopharm.* **2017**, *115*, 52–64. https://doi.org/10.1016/j.ejpb.2017.02.015.
23. Yu, P.; Han, X.; Yin, L.; Hui, K.; Guo, Y.; Yuan, A.; Hu, Y.; Wu, J. Artificial Red Blood Cells Constructed by Replacing Heme with Perfluorodecalin for Hypoxia-Induced Radioresistance. *Adv Ther Weinh* **2019**, *2*, 1900031. https://doi.org/10.1002/adtp.201900031.
24. Latson, G.W. Perftoran (Vidaphor)—Introduction to Western Medicine. *Shock* **2019**, *52*, 65–69. https://doi.org/10.1097/SHK.0000000000001063.
25. Horvat, C.M.; Carcillo, J.A.; Dezfulian, C. Liquid Fluorocarbon Lavage to Clear Thrombus from the Distal Airways after Severe Pulmonary Hemorrhage Requiring Extracorporeal Life Support (ECLS). *Respir. Med. Case Rep.* **2015**, *15*, 7–8. https://doi.org/10.1016/j.rmcr.2015.02.010.
26. Caridi-Scheible, M.E.; Blum, J.M. Use of Perfluorodecalin for Bronchoalveolar Lavage in Case of Severe Pulmonary Hemorrhage and Extracorporeal Membrane Oxygenation. *A A Case Rep.* **2016**, *7*, 215–218. https://doi.org/10.1213/XAA.0000000000000389.
27. Church, J.T.; Perkins, E.M.; Coughlin, M.A.; McLeod, J.S.; Boss, K.; Bentley, J.K.; Hershenson, M.B.; Rabah, R.; Bartlett, R.H.; Mychaliska, G.B. Perfluorocarbons Prevent Lung Injury and Promote Development during Artificial Placenta Support in Extremely Premature Lambs. *Neonatology* **2018**, *113*, 313–321. https://doi.org/10.1159/000486387.
28. Schaschkow, A.; Mura, C.; Bietiger, W.; Peronet, C.; Langlois, A.; Bodin, F.; Dissaux, C.; Bruant-Rodier, C.; Pinget, M.; Jeandidier, N.; et al. Impact of an Autologous Oxygenating Matrix Culture System on Rat Islet Transplantation Outcome. *Biomaterials* **2015**, *52*, 180–188. https://doi.org/10.1016/j.biomaterials.2015.02.031.
29. Lee, S.; Park, H.; Yang, Y.; Lee, E.; Kim, J.; Khang, G.; Yoon, K. Improvement of Islet Function and Survival by Integration of Perfluorodecalin into Microcapsules in Vivo and in Vitro. *J. Tissue Eng. Regen. Med.* **2018**, *12*, e2110–e2122. https://doi.org/10.1002/term.2643.
30. Roberts, T.R.; Leslie, D.C.; Cap, A.P.; Cancio, L.C.; Batchinsky, A.I. Tethered-liquid Omniphobic Surface Coating Reduces Surface Thrombogenicity, Delays Clot Formation and Decreases Clot Strength Ex Vivo. *J. Biomed. Mater. Res. B Appl. Biomater.* **2020**, *108*, 496–502. https://doi.org/10.1002/jbm.b.34406.
31. Suvarnapathaki, S.; Ramos, R.; Sawyer, S.W.; McLoughlin, S.; Ramos, A.; Venn, S.; Soman, P. Generation of Cell-Laden Hydrogel Microspheres Using 3D Printing-Enabled Microfluidics. *J. Mater. Res.* **2018**, *33*, 2012–2018. https://doi.org/10.1557/jmr.2018.77.
32. Ramajayam, K.K.; Kumar, A.; Sarangi, S.K.; Thirugnanam, A. A Study on Improving the Outcome of Cryosurgery Using Low Thermal Conductivity Emulsions. *Heat. Mass. Transf.* **2018**, *54*, 3727–3738. https://doi.org/10.1007/s00231-018-2397-0.
33. Elg, D.T.; Graves, D.B. Perfluorodecalin to Enhance Reactive Species Delivery in Plasma-Biomaterial Interactions. *J. Phys. D Appl. Phys.* **2019**, *52*, 355204. https://doi.org/10.1088/1361-6463/ab2a62.
34. Gold, M.H.; Nestor, M.S. A Supersaturated Oxygen Emulsion for Wound Care and Skin Rejuvenation. *J. Drugs Dermatol.* **2020**, *19*, 250–253.
35. Reddy, K.K.; Brauer, J.A.; Anolik, R.; Bernstein, L.; Brightman, L.; Hale, E.; Karen, J.; Weiss, E.; Geronemus, R.G. Topical Perfluorodecalin Resolves Immediate Whitening Reactions and Allows Rapid Effective Multiple Pass Treatment of Tattoos. *Lasers Surg. Med.* **2013**, *45*, 76–80. https://doi.org/10.1002/lsm.22106.
36. Bernstein, E.F. Commentary: On Biesman et al. Rapid, High-Fluence Multi-Pass Q-Switched Laser Treatment of Tattoos with a Transparent Perfluorodecalin-Infused Patch: A Pilot Study. *Lasers Surg. Med.* **2015**, *47*, 619–619. https://doi.org/10.1002/lsm.22408.
37. Biesman, B.S.; O'Neil, M.P.; Costner, C. Rapid, High-fluence Multi-pass Q-switched Laser Treatment of Tattoos with a Transparent Perfluorodecalin-infused Patch: A Pilot Study. *Lasers Surg. Med.* **2015**, *47*, 613–618. https://doi.org/10.1002/lsm.22399.
38. Torbeck, R.L.; Saedi, N. Optimization of Laser Tattoo Removal: Optical Clearing Agents and Multiple Same-Day Treatments via the R0 and R20 Methods. *Curr. Dermatol. Rep.* **2016**, *5*, 136–141. https://doi.org/10.1007/s13671-016-0139-4.
39. Naga, L.I.; Alster, T.S. Laser Tattoo Removal: An Update. *Am. J. Clin. Dermatol.* **2017**, *18*, 59–65. https://doi.org/10.1007/s40257-016-0227-z.
40. Jeon, H.; Brightman, L.A.; Geronemus, R.G. Laser Clinical and Practice Pearls. In *Lasers in Dermatology and Medicine*; Springer International Publishing: Cham, Switzerland, 2018; pp. 401–414.
41. Vangipuram, R.; Hamill, S.S.; Friedman, P.M. Accelerated Tattoo Removal with Acoustic Shock Wave Therapy in Conjunction with a Picosecond Laser. *Lasers Surg. Med.* **2018**, *50*, 890–892. https://doi.org/10.1002/lsm.22945.
42. Costner, C.; Biesman, B.S. Commentary on Safety of Perfluorodecalin-Infused Silicone Patch in Picosecond Laser-Assisted Tattoo Removal. *Dermatol. Surg.* **2019**, *45*, 296–298. https://doi.org/10.1097/DSS.0000000000001795.

43. Feng, H.; Geronemus, R.G.; Brauer, J.A. Safety of a Perfluorodecalin-Infused Silicone Patch in Picosecond Laser-Assisted Tattoo Removal: A Retrospective Review. *Dermatol. Surg.* **2019**, *45*, 618–621. https://doi.org/10.1097/DSS.0000000000001522.
44. Danysz, W.; Becker, B.; Begnier, M.; Clermont, G.; Kreymerman, P. The Effect of the Perfluorodecalin Patch on Particle Emission and Skin Temperature during Laser-Induced Tattoo Removal. *J. Cosmet. Laser Ther.* **2020**, *22*, 150–158. https://doi.org/10.1080/14764172.2020.1774061.
45. Paquet, P.; Fischer, M.T.; Distelmaier, P.; Mammen, A.; Meyer, L.M.; Schönfeld, C.-L. Bilateral Simultaneous Retinal Detachment in Pseudophakia. *Case Rep. Ophthalmol.* **2015**, *6*, 298–300. https://doi.org/10.1159/000439374.
46. Joussen, A.M.; Wong, D. Egress of Large Quantities of Heavy Liquids from Exposed Choroid: A Route for Possible Tumor Dissemination via Vortex Veins in Endoresection of Choroidal Melanoma. *Graefe'S Arch. Clin. Exp. Ophthalmol.* **2015**, *253*, 177–178. https://doi.org/10.1007/s00417-014-2911-0.
47. Zhmuryk, D.; Khramenko, N.; Slobodyanik, S.; Miliienko, M. Effect of Two Week Tamponade Using Perfluorocarbon Liquid and Light Silicone Oil on the Bioelectrical Functional Activity in the Retina in Rabbits. *Oftalmol. Zh* **2016**, *60*, 37–40. https://doi.org/10.31288/oftalmolzh201623740.
48. Schwartz, S.; Vaziri, K.; Kishor, K.; Flynn, H. Tamponade in the Surgical Management of Retinal Detachment. *Clin. Ophthalmol.* **2016**, *10*, 471. https://doi.org/10.2147/OPTH.S98529.
49. Dal Vecchio, M.; Fea, A.M.; Spinetta, R.; Marasso, S.L.; Cocuzza, M.; Scaltrito, L.; Canavese, G. *Behaviour of the Intraocular Pressure during Manual and Vented Gas Forced Infusion in a Simulated Pars Plana Vitrectomy*; Academic Press: Cambridge, MA, USA, 2017; Volume 12.
50. Papastavrou, V.T.; Chatziralli, I.; McHugh, D. Gas Tamponade for Retinectomy in PVR-Related Retinal Detachments: A Retrospective Study. *Ophthalmol. Ther.* **2017**, *6*, 161–166. https://doi.org/10.1007/s40123-017-0078-6.
51. Liu, W.; Gao, M.; Liang, X. Management of Subfoveal Perfluorocarbon Liquid: A Review. *Ophthalmologica* **2018**, *240*, 1–7. https://doi.org/10.1159/000488118.
52. Caporossi, T.; Tartaro, R.; Finocchio, L.; Barca, F.; Giansanti, F.; Franco, F.; Rizzo, S. Perfluorodecalin Versus Densiron 68 Heavy Silicone Oil in the Management of Inferior Retinal Detachment Recurrence. *Ophthalmic Surg. Lasers Imaging Retin.* **2019**, *50*, 274–280. https://doi.org/10.3928/23258160-20190503-03.
53. Arslanov, G.M.; Aznabaev, B.M.; Mukhamadeev, T.R.; Yanbukhtina, Z.R.; Dibaev, T.I.; Shakirova, G.R. Electron Microscopic Retina Changes in Rabbit Eyes with Perfluorocarbon Liquids Intravitreal Tamponade. *Ophthalmol. Russ.* **2019**, *16*, 81–87. https://doi.org/10.18008/1816-5095-2019-1-81-87.
54. Frolychev, I.A.; Pashtaev, N.P.; Pozdeyeva, N.A.; Sycheva, D.V. Efficacy of Tamponade of Vitreal Cavity by Perfluororganic Compound Emulsion with Antibiotics Solutions in Treatment of Gram Negative Endopthalmitis (Experimental Study). *Ophthalmol. Russ.* **2019**, *16*, 494–500. https://doi.org/10.18008/1816-5095-2019-4-494-500.
55. Caporossi, T.; De Angelis, L.; Pacini, B.; Rizzo, S. Amniotic Membrane for Retinal Detachment Due to Paravascular Retinal Breaks over Patchy Chorioretinal Atrophy in Pathologic Myopia. *Eur. J. Ophthalmol.* **2020**, *30*, 392–395. https://doi.org/10.1177/1120672119891415.
56. Natchimuthu, V.; Thomas, S.; Ramalingam, M.; Ravi, S. Improved Performance of Antiepileptic Drugs by Oxygen Enrichment Through Perfluorodecalin in Nanoscales. *Adv. Sci. Lett.* **2016**, *22*, 745–751. https://doi.org/10.1166/asl.2016.6931.
57. Natchimuthu, V.; Jayalatha, K.A.; Ravi, S. Characterizing the Molecular Interaction of Perfluorocarbons with Carbamazepine and Benzodiazepine Using Photo-Acoustic Studies. *J. Mol. Liq.* **2016**, *218*, 120–127. https://doi.org/10.1016/j.molliq.2016.02.038.
58. Natchimuthu, V.; Thomas, S.; Ramalingam, M.; Ravi, S. Influence of Perfluorocarbons on Carbamazepine and Benzodiazepine for a Neuro-Lung Protective Strategy. *J. Clin. Neurosci.* **2017**, *43*, 82–88. https://doi.org/10.1016/j.jocn.2017.04.019.
59. Chen, G.; Wang, K.; Wu, P.; Wang, Y.; Zhou, Z.; Yin, L.; Sun, M.; Oupický, D. Development of Fluorinated Polyplex Nanoemulsions for Improved Small Interfering RNA Delivery and Cancer Therapy. *Nano Res.* **2018**, *11*, 3746–3761. https://doi.org/10.1007/s12274-017-1946-z.
60. Natchimuthu, V.; Ravi, S.; Amoros, J. Effect of Sonication on Certain Antiepileptic Drugs: Approach to Drug Delivery Mechanism Through Perfluorocarbon. *Asian J. Chem.* **2019**, *31*, 417–421. https://doi.org/10.14233/ajchem.2019.21669.
61. Giuliani, N.; Saugy, M.; Augsburger, M.; Varlet, V. Blood Monitoring of Perfluorocarbon Compounds (F-Tert-Butylcyclohexane, Perfluoromethyldecalin and Perfluorodecalin) by Headspace-Gas Chromatography-Tandem Mass Spectrometry. *Talanta* **2015**, *144*, 196–203. https://doi.org/10.1016/j.talanta.2015.05.015.
62. Sun, S.; Buer, B.C.; Marsh, E.N.G.; Kennedy, R.T. A Label-Free Sirtuin 1 Assay Based on Droplet-Electrospray Ionization Mass Spectrometry. *Anal. Methods* **2016**, *8*, 3458–3465. https://doi.org/10.1039/C6AY00698A.
63. Gulyaev, M.V.; Kuznetsova, A.V.; Silachev, D.N.; Danilina, T.I.; Gervits, L.L.; Pirogov, Y.A. Realization of 19F MRI Oximetry Method Using Perfluorodecalin. *Magn. Reson. Mater. Phys. Biol. Med.* **2019**, *32*, 307–315. https://doi.org/10.1007/s10334-019-00739-1.
64. Sykłowska-Baranek, K.; Pilarek, M.; Bonfill, M.; Kafel, K.; Pietrosiuk, A. Perfluorodecalin-Supported System Enhances Taxane Production in Hairy Root Cultures of Taxus x Media Var. Hicksii Carrying a Taxadiene Synthase Transgene. *Plant Cell Tissue Organ Cult. (PCTOC)* **2015**, *120*, 1051–1059. https://doi.org/10.1007/s11240-014-0659-1.
65. Vieira, E.S.; de Oliveira Fontes, T.K.; Pereira, M.M.; Alexandre, H.V.; da Silva, D.P.; Soares, C.M.F.; Lima, Á.S. New Strategy to Apply Perfluorodecalin as an Oxygen Carrier in Lipase Production: Minimisation and Reuse. *Bioprocess. Biosyst. Eng.* **2015**, *38*, 721–728. https://doi.org/10.1007/s00449-014-1312-4.

66. Pilarek, M.; Dąbkowska, K. Modelling of a Hybrid Culture System with a Stationary Layer of Liquid Perfluorochemical Applied as Oxygen Carrier. *Chem. Process Eng.* **2016**, *37*, 149–158. https://doi.org/10.1515/cpe-2016-0014.
67. Sutoh, A.; Kasuya, M.C.Z.; Hatanaka, K. Cellular Glycosylation of Amphiphilic Saccharide Primer in Liquid/Liquid Interface Culture System Employing Fluorous Solvents. *J. Fluor. Chem.* **2016**, *188*, 76–79. https://doi.org/10.1016/j.jfluchem.2016.06.011.
68. Vidal-Limon, H.R.; Almagro, L.; Moyano, E.; Palazon, J.; Pedreño, M.A.; Cusido, R.M. Perfluorodecalins and Hexenol as Inducers of Secondary Metabolism in Taxus Media and Vitis Vinifera Cell Cultures. *Front. Plant Sci.* **2018**, *9*, 335. https://doi.org/10.3389/fpls.2018.00335.
69. Westbrook, A.W.; Ren, X.; Moo-Young, M.; Chou, C.P. Application of Hydrocarbon and Perfluorocarbon Oxygen Vectors to Enhance Heterologous Production of Hyaluronic Acid in Engineered *Bacillus Subtilis*. *Biotechnol. Bioeng.* **2018**, *115*, 1239–1252. https://doi.org/10.1002/bit.26551.
70. Miyajima, H.; Kasuya, M.C.Z.; Hatanaka, K. New Fluorous Gelators for Perfluorodecalin. *J. Fluor. Chem.* **2019**, *222–223*, 24–30. https://doi.org/10.1016/j.jfluchem.2019.04.008.
71. Kirchhelle, C.; Moore, I. A Simple Chamber for Long-Term Confocal Imaging of Root and Hypocotyl Development. *J. Vis. Exp.* **2017**, *17*, 55331. https://doi.org/10.3791/55331.
72. Sykłowska-Baranek, K.; Łysik, K.; Jeziorek, M.; Wencel, A.; Gajcy, M.; Pietrosiuk, A. Lignan Accumulation in Two-Phase Cultures of Taxus x Media Hairy Roots. *Plant Cell Tissue Organ Cult. (PCTOC)* **2018**, *133*, 371–384. https://doi.org/10.1007/s11240-018-1390-0.
73. Sykłowska-Baranek, K.; Szala, K.; Pilarek, M.; Orzechowski, R.; Pietrosiuk, A. A Cellulase-Supported Two-Phase in Situ System for Enhanced Biosynthesis of Paclitaxel in Taxus × Media Hairy Roots. *Acta Physiol. Plant* **2018**, *40*, 201. https://doi.org/10.1007/s11738-018-2777-6.
74. Sykłowska-Baranek, K.; Rymaszewski, W.; Gaweł, M.; Rokicki, P.; Pilarek, M.; Grech-Baran, M.; Hennig, J.; Pietrosiuk, A. Comparison of Elicitor-Based Effects on Metabolic Responses of Taxus × Media Hairy Roots in Perfluorodecalin-Supported Two-Phase Culture System. *Plant Cell Rep.* **2019**, *38*, 85–99. https://doi.org/10.1007/s00299-018-2351-0.
75. Li, S.; Zhu, J.; Wang, G.; Ni, L.; Zhang, Y.; Green, C.T. Rapid Removal of Nitrobenzene in a Three-Phase Ozone Loaded System with Gas–Liquid–Liquid. *Chem. Eng. Commun.* **2015**, *202*, 799–805. https://doi.org/10.1080/00986445.2013.867259.
76. Hong, M.; Yan, J. Synthesis of *Meso*-Tetraarylporphyrins Using Hafnium (IV) Bis(Perfluorooctanesulfonyl)Imide Complex in Perfluorodecalin Medium. *J. Chem. Res.* **2016**, *40*, 549–551. https://doi.org/10.3184/174751916X14718751882863.
77. Rodriguez-Brotons, A.; Bietiger, W.; Peronet, C.; Langlois, A.; Magisson, J.; Mura, C.; Sookhareea, C.; Polard, V.; Jeandidier, N.; Zal, F.; et al. Comparison of Perfluorodecalin and HEMOXCell as Oxygen Carriers for Islet Oxygenation in an In Vitro Model of Encapsulation. *Tissue Eng. Part. A* **2016**, *22*, 1327–1336. https://doi.org/10.1089/ten.tea.2016.0064.
78. Grubb, M.P.; Coulter, P.M.; Marroux, H.J.B.; Orr-Ewing, A.J.; Ashfold, M.N.R. Unravelling the Mechanisms of Vibrational Relaxation in Solution. *Chem. Sci.* **2017**, *8*, 3062–3069. https://doi.org/10.1039/C6SC05234G.
79. Sokolov, V.I.; Boyko, V.E.; Goriachuk, I.O.; Igumnov, S.M.; Molchanova, S.I.; Pogodina, Y.E.; Polunin, E.V. Synthesis and Study of Optical Properties of Copolymers of Perfluoro-2,2-Dimethyl-1,3-Dioxole and Perfluoro(Propyl Vinyl Ether). *Russ. Chem. Bull.* **2017**, *66*, 1284–1289. https://doi.org/10.1007/s11172-017-1886-5.
80. Jalani, G.; Jeyachandran, D.; Bertram Church, R.; Cerruti, M. Graphene Oxide-Stabilized Perfluorocarbon Emulsions for Controlled Oxygen Delivery. *Nanoscale* **2017**, *9*, 10161–10166. https://doi.org/10.1039/C7NR00378A.
81. Song, B.; Hu, K.; Qin, A.; Tang, B.Z. Oxygen as a Crucial Comonomer in Alkyne-Based Polymerization toward Functional Poly(Tetrasubstituted Furan)s. *Macromolecules* **2018**, *51*, 7013–7018. https://doi.org/10.1021/acs.macromol.8b01293.
82. Baranov, D.; Toso, S.; Imran, M.; Manna, L. Investigation into the Photoluminescence Red Shift in Cesium Lead Bromide Nanocrystal Superlattices. *J. Phys. Chem. Lett.* **2019**, *10*, 655–660. https://doi.org/10.1021/acs.jpclett.9b00178.
83. Kambur, P.S.; Pashkevich, D.S.; Petrov, V.B.; Alekseev, Y.I.; Yampol'skii, Y.P.; Alent'ev, A.Y. Gas-Liquid Fluorination of 1,1,1,2-Tetrafluoroethane and Methane with Elemental Fluorine in a Perfluorinated Liquid. *Russ. J. Appl. Chem.* **2019**, *92*, 958–963. https://doi.org/10.1134/S1070427219070127.
84. Miller, M.A.; Day, R.A.; Estabrook, D.A.; Sletten, E.M. A Reduction-Sensitive Fluorous Fluorogenic Coumarin. *Synlett* **2020**, *31*, 450–454. https://doi.org/10.1055/s-0039-1690770.
85. May-Masnou, A.; Stébé, M.J.; Blin, J.L. Hierarchical Meso-Mesoporous and Macro-Mesoporous Silica Templated by Mixtures of Polyoxyethylene Fluoroalkyl Ether and Triblock Copolymer. *Eur. J. Inorg. Chem.* **2016**, *2016*, 1998–2005. https://doi.org/10.1002/ejic.201501168.
86. Tian, B.; Yang, B.; Li, J.; Li, Z.; Zhen, W.; Wu, Y.; Lu, G. Water Splitting by CdS/Pt/WO 3-CeO x Photocatalysts with Assisting of Artificial Blood Perfluorodecalin. *J. Catal.* **2017**, *350*, 189–196. https://doi.org/10.1016/j.jcat.2017.03.012.
87. Gao, W.; Zhang, W.; Lu, G. A Two-Pronged Strategy to Enhance Visible-Light-Driven Overall Water Splitting via Visible-to-Ultraviolet Upconversion Coupling with Hydrogen-Oxygen Recombination Inhibition. *Appl. Catal. B* **2017**, *212*, 23–31. https://doi.org/10.1016/j.apcatb.2017.04.063.
88. Tian, B.; Gao, W.; Zhang, X.; Wu, Y.; Lu, G. Water Splitting over Core-Shell Structural Nanorod CdS@Cr_2O_3 Catalyst by Inhibition of H2-O2 Recombination via Removing Nascent Formed Oxygen Using Perfluorodecalin. *Appl. Catal. B* **2018**, *221*, 618–625. https://doi.org/10.1016/j.apcatb.2017.09.065.
89. Lee, J.W.; Yu, H.; Lee, K.; Bae, S.; Kim, J.; Han, G.R.; Hwang, D.; Kim, S.K.; Jang, J. Highly Crystalline Perovskite-Based Photovoltaics via Two-Dimensional Liquid Cage Annealing Strategy. *J. Am. Chem. Soc.* **2019**, *141*, 5808–5814. https://doi.org/10.1021/jacs.8b13423.

90. Dias, A.M.A.; Gonçalves, C.M.B.; Caço, A.I.; Santos, L.M.N.B.F.; Piñeiro, M.M.; Vega, L.F.; Coutinho, J.A.P.; Marrucho, I.M. Densities and Vapor Pressures of Highly Fluorinated Compounds. *J. Chem. Eng. Data* **2005**, *50*, 1328–1333. https://doi.org/10.1021/je050056e.
91. Bernardogil, G.S.; Soares, L.J.S. Mutual Binary Solubilities—Perfluorodecalin Hydrocarbons. *J. Chem. Eng. Data* **1987**, *32*, 327–329. https://doi.org/10.1021/je00049a014.
92. Bernardogil, G.; Soares, L.J.S. Liquid Liquid Equilibria for the System Perfluorodecalin/1-Heptene/n-Heptane/n-Hexane. *J. Chem. Eng. Data* **1989**, *34*, 103–106. https://doi.org/10.1021/je00055a030.
93. Maeda, N. Nucleation Curves of Model Natural Gas Hydrates on a Quasi-Free Water Droplet. *AIChE J.* **2015**, *61*, 2611–2617. https://doi.org/10.1002/aic.14898.
94. Maeda, N. Nucleation Curves of Methane—Propane Mixed Gas Hydrates in Hydrocarbon Oil. *Chem. Eng. Sci.* **2016**, *155*, 1–9. https://doi.org/10.1016/j.ces.2016.07.047.
95. Sun, S.; Zawatzky, K.; Regalado, E.L.; Mangion, I.K.; Welch, C.J. Are Fluorine-Rich Pharmaceuticals Lost by Partition into Fluorous Phases? *J. Pharm. Biomed. Anal.* **2016**, *128*, 106–110. https://doi.org/10.1016/j.jpba.2016.05.025.
96. Tremper, K.K.; Zaccari, J.; Cullen, B.F.; Hufstedler, S.M. Liquid Gas Partition-Coefficients of Halothane and Isoflurane in Perfluorodecalin, Fluosol-DA, and Blood Fluosol-DA Mixtures. *Anesth. Analg.* **1984**, *63*, 690–692.
97. Liang, K.N.; Nie, C.S. The Solubilities of Nitrogen, Oxygen and Carbon-Dioxide in Tri (Perfluoro-Propyl) Amine (FTPA) and Perfluorodecalin (FDC) at Elevated Pressures and Ambient-Temperature. *Acta Chim. Sin.* **1989**, *47*, 60–63.
98. ZareNezhad, B.; Aminian, A. Accurate Prediction of Two-Phase Behavior of the Mixtures of Carbon Dioxide and Different Perfluoroalkane Compounds: Comparison of the Presented Neuro-Fuzzy Model with Advanced Soft-SAFT Molecular Model. *Chem. Eng. Commun.* **2015**, *202*, 843–849. https://doi.org/10.1080/00986445.2013.867263.
99. Moshnyaga, A.V.; Khoroshilov, A.V.; Selivanova, D.I.; Aksenova, D.M. Thermodynamics of Dissolved Nitrogen, Nitrous Oxide, and Ammonia in Perfluorodecalin. *Russ. J. Phys. Chem. A* **2017**, *91*, 2117–2120. https://doi.org/10.1134/S0036024417100260.
100. Coelho, F.M.B.; Botelho, A.M.; Ivo, O.F.; Amaral, P.F.F.; Ferreira, T.F. Volumetric Mass Transfer Coefficient for Carbon Monoxide in a Dual Impeller Stirred Tank Reactor Considering a Perfluorocarbon–Water Mixture as Liquid Phase. *Chem. Eng. Res. Des.* **2019**, *143*, 160–169. https://doi.org/10.1016/j.cherd.2019.01.013.
101. Deepika, D.; Pandey, S. Density and Dynamic Viscosity of Perfluorodecalin-Added n-Hexane Mixtures: Deciphering the Role of Fluorous Liquids. *Liquids* **2023**, *3*, 48–56. https://doi.org/10.3390/liquids3010005.
102. Moshnyaga, A.V.; Khoroshilov, A.V.; Semyashkin, M.P.; Mel'nikov, V.V. Density of N2O Solutions in Perfluorodecalin As a Function of Concentration. *Russ. J. Phys. Chem. A* **2018**, *92*, 719–723. https://doi.org/10.1134/S0036024418040222.
103. Freire, M.G.; Ferreira, A.G.M.; Fonseca, I.M.A.; Marrucho, I.M.; Coutinho, J.A.P. Viscosities of Liquid Fluorocompounds. *J. Chem. Eng. Data* **2008**, *53*, 538–542. https://doi.org/10.1021/je700632z.
104. Haszeldine, R.N.; Smith, F. 129. Organic Fluorides. Part VI. The Chemical and Physical Properties of Certain Fluorocarbons. *J. Chem. Soc.* **1951**, *VI*, 603. https://doi.org/10.1039/jr9510000603.
105. Freire, M.G.; Carvalho, P.J.; Queimada, A.J.; Marrucho, I.M.; Coutinho, J.A.P. Surface Tension of Liquid Fluorocompounds. *J. Chem. Eng. Data* **2006**, *51*, 1820–1824. https://doi.org/10.1021/je060199g.
106. Nishikido, N.; Mahler, W.; Mukerjee, P. Interfacial-Tensions of Perfluorohexane and Perfluorodecalin against Water. *Langmuir* **1989**, *5*, 227–229. https://doi.org/10.1021/la00085a043.
107. Bąk, A.; Pilarek, M.; Podgórska, W.; Markowska-Radomska, A.; Hubacz, R. Surface Properties Ofperfluorodecalin–Containing Liquid/Liquid Systems: The Influence of Pluronic F-68 Dissolved in the Aqueous Phase. *J. Fluor. Chem.* **2018**, *215*, 36–43. https://doi.org/10.1016/j.jfluchem.2018.09.002.
108. Lhermerout, R.; Davitt, K. Contact Angle Dynamics on Pseudo-Brushes: Effects of Polymer Chain Length and Wetting Liquid. *Colloids Surf. A Physicochem. Eng. Asp.* **2019**, *566*, 148–155. https://doi.org/10.1016/j.colsurfa.2019.01.006.
109. Delpuech, J.J.; Mathis, G.; Ravey, J.C.; Selve, C.; Serratrice, G.; Stebe, M.J. Perfluorodecalin as a Carrier of Respiratory Gases—Preparation and Physicochemical Properties of Their Aqueous Microemulsions. *Bull. Soc. Chim. Fr.* **1985**, *122*, 578–581.
110. Jochyms, Q.; Guillot, P.; Mignard, E.; Vincent, J.-M. A Fluorosurfactant and Photoreducible Cu^{II}-Tren Click Catalyst: Surfactant and Catalytic Properties at Liquid/Liquid Interfaces. *Dalton Trans.* **2015**, *44*, 19700–19707. https://doi.org/10.1039/C5DT02039E.
111. Kumacheva, E.E.; Amelina, E.A.; Popov, V.I. Effect of Flocculation on Enlargement of Particles of Aqueous Emulsions of Perfluorodecalin. *Colloid J. Ussr* **1989**, *51*, 1057–1058.
112. Tovar, T.M.; Mahle, J.J.; Knox, C.K.; LeVan, M.D. 110th Anniversary: Molecular Structure Effects on Mass Transfer of C_{10} Hydrocarbons in BPL Activated Carbon. *Ind. Eng. Chem. Res.* **2019**, *58*, 15271–15279. https://doi.org/10.1021/acs.iecr.9b02377.
113. Aramendia, I.; Fernandez-Gamiz, U.; Lopez-Arraiza, A.; Rey-Santano, C.; Mielgo, V.; Basterretxea, F.; Sancho, J.; Gomez-Solaetxe, M. Experimental and Numerical Modeling of Aerosol Delivery for Preterm Infants. *Int. J. Env. Res. Public. Health* **2018**, *15*, 423. https://doi.org/10.3390/ijerph15030423.
114. Mack, H.G.; Oberhammer, H. The Gas-Phase Structures of Trans-Perfluorodecalin and Cis-Perfluorodecalin. *J. Mol. Struct.* **1989**, *197*, 321–328. https://doi.org/10.1016/0022-2860(89)85172-5.
115. Le Bris, K.; DeZeeuw, J.; Godin, P.J.; Strong, K. Cis- and Trans-Perfluorodecalin: Infrared Spectra, Radiative Efficiency and Global Warming Potential. *J. Quant. Spectrosc. Radiat. Transf.* **2017**, *203*, 538–541. https://doi.org/10.1016/j.jqsrt.2017.01.011.
116. Fung, B.M. Selective Derection of Multiplets via Double Quantum Coherence—A F-19-NMR Study of Perfluorodecalin. *Org. Magn. Reson.* **1983**, *21*, 397–398. https://doi.org/10.1002/omr.1270210612.

117. Dobychin, S.L.; Turkina, M.Y.; Kalinina, N.M. Mass-Spectra and Metastable Decays of Perfluorodecalin Isomers and Its Trifluoromethyl Derivatives. *Zhurnal Org. Khimii* **1983**, *19*, 2572–2577.
118. Jacoby, C.; Temme, S.; Mayenfels, F.; Benoit, N.; Krafft, M.P.; Schubert, R.; Schrader, J.; Flögel, U. Probing Different Perfluorocarbons for in Vivo Inflammation Imaging by ^{19}F MRI: Image Reconstruction, Biological Half-Lives and Sensitivity. *NMR Biomed.* **2014**, *27*, 261–271. https://doi.org/10.1002/nbm.3059.
119. Gervits, L.L.; Snegirov, V.F.; Makarov, K.N.; Galakhov, M.V.; Mukhin, V.Y. Non-Chair Conformation of Cis Isomers of 1,4-Disubstituted Perfluorocyclohexanes. *Bull. Acad. Sci. USSR Div. Chem. Sci.* **1987**, *36*, 2664–2665. https://doi.org/10.1007/BF00957267.
120. Sereda, S.V.; Gervits, L.L.; Antipin, M.Y.; Makarov, K.N.; Struchkov, Y.T. Molecular and Crystal Structure of Derivatives of Higher Internal Perfluoroalkenes. *J. Struct. Chem.* **1989**, *30*, 349–353. https://doi.org/10.1007/BF00761331.
121. Platonov, V.E.; Dvornikova, K.V.; Prokudin, I.P.; Melnichenko, B.A.; Yakobson, G.G. Isomerization of Cis-Perfluorodecalin and Trans-Perfluorodecalin. *Bull. Acad. Sci. Ussr Div. Chem. Sci.* **1985**, *34*, 224. https://doi.org/10.1007/BF01157370.
122. Petrov, A.A. *Stereochemistry of Saturated Hydrocarbons*; Nauka: Moscow, Russia, 1981.
123. Smith, B.J.; Patrick, C.R. Cis-and Trans-Perfluorodecalin. *Proc. Chem. Soc. Lond*. **1961**, *4*, 138.
124. Homer, J.; Thomas, L.F. The Nuclear Magnetic Resonance Spectra of Cis- and Trans-Perfluorodecalin. *Proc. Chem. Soc.* **1961**, 139–140. https://doi.org/10.1039/PS9610000129.
125. Brandenburg, T.; Petit, T.; Neubauer, A.; Atak, K.; Nagasaka, M.; Golnak, R.; Kosugi, N.; Aziz, E.F. Fluorination-Dependent Molecular Orbital Occupancy in Ring-Shaped Perfluorocarbons. *Phys. Chem. Chem. Phys.* **2015**, *17*, 18337–18343. https://doi.org/10.1039/C5CP01254F.
126. Zhalimov, V.; Sklifas, A.; Kaptsov, V.; Penkov, N.; Temnov, A.; Kukushkin, N. The Chemical Structure of Triblock Copolymers and the Adsorption Capacity of Perfluorocarbon—Core Nanoparticles Stabilized by Them. *Colloid. Polym. Sci.* **2018**, *296*, 251–257. https://doi.org/10.1007/s00396-017-4245-z.
127. Kambur, P.S.; Pashkevich, D.S.; Alekseev, Y.I.; Yampolskii, Y.P.; Alentev, A.Y. Interaction of Perfluorinated Fluids with Fluorine in Gas-Liquid Reactor. *Russ. J. Appl. Chem.* **2019**, *92*, 661–666. https://doi.org/10.1134/S1070427219050124.
128. Mattsson, S.; Paulus, B.; Redeker, F.A.; Beckers, H.; Riedel, S.; Müller, C. The Crystal Structure of A-F_2 : Solving a 50 Year Old Puzzle Computationally. *Chem. A Eur. J.* **2019**, *25*, 3318–3324. https://doi.org/10.1002/chem.201805300.
129. Tantardini, C.; Jalolov, F.N.; Kvashnin, A.G. Crystal Structure Evolution of Fluorine under High Pressure. *J. Phys. Chem. C* **2022**, *126*, 11358–11364. https://doi.org/10.1021/acs.jpcc.2c02213.
130. Polkovnichenko, A.V.; Lupachev, E.V.; Kisel', A.V.; Kvashnin, S.Y.; Kulov, N.N. Perfluoro(7-Methylbicyclo [4.3.0]Nonane) and Perfluoro(Butylcyclohexane): Physicochemical, Thermophysical, and Spectral Data. *J. Chem. Eng. Data* **2023**, *68*, 499–517. https://doi.org/10.1021/acs.jced.2c00588.
131. Polkovnichenko, A.V.; Lupachev, E.V.; Kisel', A.V.; Kvashnin, S.Y.; Kulov, N.N. Perfluoro(7-Methylbicyclo [4.3.0]Nonane) Purification from Close-Boiling Impurities by Heteroazeotropic Distillation Method. In Proceedings of the 2nd International Electronic Conference on Processes: Process Engineering—Current State and Future Trends (ECP 2023), Online, 17–31 May 2023; p. 72.
132. Kisel, A.V.; Polkovnichenko, A.V.; Lupachev, E.V.; Kuritsyn, N.N.; Kvashnin, S.Y.; Kulov, N.N. The Process of Isolation, Using Crystallization of Cis- and Trans-Isomers, of Perfluorodecalines from an Industrial Mixture of Electrochemical Fluorination of Napthaline. In Proceedings of the ECP 2023, Online, 17 May 2023; p. 85.
133. Polkovnichenko, A.V.; Lupachev, E.V.; Kisel', A.V.; Kvashnin, S.Y.; Kulov, N.N. Separation of an Industrial Mixture of Decalin or Naphthalene Fluorination Products. Purification of Perfluoro(7-Methylbicyclo[4.3.0]Nonane) from Close-Boiling Impurities by Heteroazeotropic Distillation. *Theor. Found. Chem. Eng.* **2023**, *57*, 779-790. https://doi.org/10.1134/S0040579523050500.
134. Polkovnichenko, A.V.; Kulov, N.N.; Kisel', A.V.; Kuritsyn, N.N.; Kvashnin, S.Y.; Lupachev, E.V. Separation of an Industrial Mixture of Decalin or Naphthalene Fluorination Products. Physicochemical Foundations of Crystallization of Binary Mixtures of Cis- and Trans-Perfluorodecalin and Perfluorobutylcyclohexane. *Theor. Found. Chem. Eng*. **2023**, *57,* in press .
135. Bispen, T.A.; Kochnev, A.D.; Moldavskij, D.D.; Sergeeva, A.A. Method of Purifying Perfluorodecalin. RU 2544849 C1, 20 March 2015.
136. Gervits, L.L. Perfluorocarbon-Based Blood Substitutes Russian Experience. In Proceedings of the Fluorine in Medicine in the 21st Century 1994, Manchester, UK, 18–21 April 1994; Paper 22, pp. 1–9.
137. Trejbal, J.; Zapletal, M.; Obuchov, A.; Sommer, T. Determination of Density, Viscosity, and Saturated Vapor Pressure of Various Itaconic Acid Esters. *Int. J. Thermophys.* **2022**, *43*, 51. https://doi.org/10.1007/s10765-022-02975-5.
138. Redlich, O.; Kister, A.T. Algebraic Representation of Thermodynamic Properties and the Classification of Solutions. *Ind. Eng. Chem.* **1948**, *40*, 345–348. https://doi.org/10.1021/ie50458a036.
139. Rodríguez, G.A.; Delgado, D.R.; Martínez, F.; Khoubnasabjafari, M.; Jouyban, A. Volumetric Properties of Some Pharmaceutical Binary Mixtures at Low Temperatures and Correlation with the Jouyban-Acree Model. *Rev. Colomb. Cienc. QuÍM. Farm.* **2011**, *40*, 222–239.
140. Kohler, F. Zur Berechnung Der Thermodynamischen Daten Eines Ternaren Systems Aus Den Zugehorigen Binaren Systemen. *Monatsh Chem.* **1960**, *91*, 738–740. https://doi.org/10.1007/BF00899814.
141. Adam, O.E.-A.A.; Awwad, A.M. Estimation of Excess Molar Volumes and Theoretical Viscosities of Binary Mixtures of Benzene + N-Alkanes at 298.15 K. *Int. J. Ind. Chem.* **2016**, *7*, 391–400. https://doi.org/10.1007/s40090-016-0100-1.

142. NIST Mass Spectrometry Data Center; William, E.W. (Dirs.) Mass Spectra. In N*IST Chemistry WebBook*; NIST Standard Reference Database Number 69; Linstrom, P.J., Mallard, W.G., Eds.; National Institute of Standards and Technology, Gaithersburg, MD, USA. Available online: https://webbook.nist.gov/cgi/inchi?ID=C60433116&Mask=200 (accessed on 18 September 2023).
143. Domalski, E.S.; Hearing, E.D. Heat Capacities and Entropies of Organic Compounds in the Condensed Phase. Volume III. *J. Phys. Chem. Ref. Data* **1996**, *25*, 1. https://doi.org/10.1063/1.555985.
144. Kanno, H. A Simple Derivation of the Empirical Rule. *J. Non Cryst. Solids* **1981**, *44*, 409–413. https://doi.org/10.1016/0022-3093(81)90047-8.
145. Varushchenko, R.M.; Druzhinina, A.I.; Pashchenko, L.L. Thermodynamics of Vaporization of Some Cyclic Perfluorocarbons. *Fluid. Phase Equilib.* **1996**, *126*, 93–104. https://doi.org/10.1016/S0378-3812(96)03111-1.
146. Chelyuskina, T.V.; Bedretdinov, F.N. Mathematical Modeling of Extractive Rectification of a Butyl Butyrate–Butyric Acid Mixture. *Theor. Found. Chem. Eng.* **2016**, *50*, 697–704. https://doi.org/10.1134/S0040579516050274.